Aminated nanocellulose-mediated synthesis of polyaniline/nanocellulose hybrid materials for sustainable conductive and supercapacitors nanopapers

Fadwa Gharsallah, Emna Ben Ayed, Nouha Ghorbel, Jean-Luc Putaux, Sami Boufi

Aminated nanocellulose-mediated synthesis of polyaniline/nanocellulose hybrid materials for sustainable conductive and supercapacitors nanopapers

Fadwa Gharsallah[1], Emna Ben Ayed[2], Nouha Ghorbel[1], Jean-Luc Putaux[3], Sami Boufi[2*]

[1]*University of Sfax, Faculty of Sciences, LaMaCoP, BP 1171, 3018 Sfax, Tunisia*

[2]*University of Sfax, Faculty of Sciences, LSME, BP 1171, 3018 Sfax, Tunisia*

[3] *Univ. Grenoble Alpes, CNRS, CERMAV, F-38000 Grenoble, France*

Corresponding authors: *sami.boufi@fss.rnu.tn* - *ghorbel_nouha@yahoo.fr*

Published in **Materials Today Sustainability** 27 (2024), 100811

DOI: 10.1016/j.mtsust.2024.100811

Abstract:

Diamine-functionalized cellulose nanocrystals (DamCNCs) prepared by periodate oxidation and reductive amination were used as a scaffold for the *in-situ* oxidative polymerization of polyaniline (PANI). Unlike unmodified CNCs, the hybrid PANI/DamCNC particles formed a stable colloidal suspension over a large pH domain, PANI particles having nucleated and grown from the nanocrystals. The hybridization of PANI was validated by transmission electron microscopy images, along with Fourier-transform infrared, Raman, and UV-Vis spectra. By taking advantage of the colloidal stability of the PANI/DamCNC nanohybrids, flexible and freestanding thin nanopapers were prepared, with different contents in PANI/DamCNCs, using cationic or anionic cellulose nanofibrils (CCNFs or ACNFs, respectively). Conductive nanopapers were obtained by mixing CCNFs with PANI/DamCNCs at a content higher than 20 wt%, exhibiting high flexibility, mechanical integrity, transparency, and stability over time. This work proposes a simple process to fabricate a novel class of biobased conductive hybrid nanofiller based on PANI grafted on DamCNCs, stable in water, that may be used as an additive in nanocellulose suspensions to produce green flexible thin nanopapers, with potential use in different types of electronic devices such as electronic displays, smart packaging, or paper-based supercapacitors for energy storage.

Abbreviations:

AGU – anydroglucose unit
ACNF – anionic cellulose nanofibril
CCNF – cationic cellulose nanofibril
ChNC – chitin nanocrystal
CNF – cellulose nanofibril
CNC – cellulose nanocrystal
NR – natural rubber
DamCNC – diaminated cellulose nanocrystal
DalCNC – dialdehyde cellulose nanocrystal
EB – emeraldine base
ES – emeraldine salt
NC – nanocellulose
NDP – never-dried pulp
PANI – polyaniline

1. INTRODUCTION

Over the last few decades, intrinsically conductive polymers have become a highly sought-after class of materials with a wide range of applications. Polyaniline (PANI) is one of the most researched intrinsically conductive polymers [1]. The nitrogen-containing heterocyclic ring structure makes it an excellent electron donor and acceptor. The frequently researched form of PANI is the emeraldine salt (ES) which has a highly ordered structure with alternating double and single bonds along its backbone. The resulting high conductivity can be further increased by doping the material with an oxidizing agent. However, PANI in its conducting form might present unsatisfactory performance due to (i) the presence of a highly conjugated π electron system and a rigid backbone which limits its ability to generate pristine PANI films by casting and evaporation method [2], (ii) insolubility and non-dispersion in water or any other conventional organic solvents [3], and (iii) relatively poor mechanical properties [4]. All these drawbacks seriously undermine the application of PANI as a potential material. Accordingly, several strategies have been proposed to overcome these limitations to some extent.

One of the most common methods is to combine PANI with polymer surfactants to generate complexes with better film-forming capabilities [5,6]. Another promising approach consists in co-blending PANI with conventional polymers to produce films with improved electrical conductivity, higher mechanical strength or by combining these two characteristics via casting/evaporation [7–10], fusion [11–13], emulsion [14,15] or inverse emulsion [16–18]. Unfortunately, these methods are not scalable due to the significant amounts of solvents involved and the presence of chemical substances that may be toxic and hard to wash out. Further, the mechanical and electrical properties of the resulting composite material may be inconsistent, as these properties are greatly influenced by the concentration and dispersion state of PANI in the matrix. An optimum dispersion is thus extremely difficult to achieve and may result in processing difficulties as well as a decrease in mechanical quality. Hence, achieving promising electrical properties through a simple doping/de-doping mechanism with small amounts of PANI while maintaining their good processability and mechanical qualities remains the key challenge to reaching the full potential of such nanocomposites that would allow extending their use in the industry.

The use of nanocelluloses (NCs) as renewable building blocks for the rational design of functional materials is now well acknowledged in several recent and past works [19–21] whether for applications in flexible electronics [22,23], energy storage [24,25], or biomedical devices [26]. With their outstanding stiffness and strength for an organic material (Young's modulus was 140 for cellulose nanocrystals (CNCs) [27], and between 20-80 GPa for cellulose nanofibrils

(CNFs) [28], respectively), flexibility, and high surface area, CNFs and CNCs, opened new opportunities for polymer-based conductors through hybridization with highly intrinsic polymer conductor, leading to the development of new and improved materials with enhanced conductivity, transparency, and durability [2,29,30]. Moreover, thanks to the presence of a high density of hydroxyl surface groups (either primary in C6 or secondary in C2, C3, and C4 of the constituting anydroglucose unit, or AGU), additional functions can be imparted via the chemistry of hydroxyl groups in cellulose such as carboxyl, aldehyde, amine, sulfate, among other functionalities [31–33].

The hybridization of nanocelluloses (CNCs, CNFs, or bacterial cellulose) with PANI has recently attracted significant attention due to the numerous merits and unique properties of this class of material, with a wide range of possibilities of application in advanced materials such as flexible electronics, energy storage, or biomedical devices. The main objective is to take advantage of each class of material to which NCs will bring mechanical properties, dispersibility, and aptitude to form thin flexible or stiff films, while PANI provides electrical properties. For instance, Wu et al. prepared an organized 3D hierarchical structure in natural rubber (NR) based nanocomposites with a low percolation threshold and high mechanical properties using CNCs as biotemplates to form PANI/CNC nanohybrids [34]. These nanocomposites showed that the electrical conductivity of PANI@CNC/NR that contained 5 parts per hundred parts of NR was 11 orders of magnitude higher compared to PANI/NR composites with the same loading fractions of PANI. Zhang et al. manufactured nanocomposite films based on core-shell PANI/NC structured material with electrochemical properties in an electrolyte solution [29]. More recently, Gopakumar et al. fabricated a series of conductive cellulose nanopapers to attenuate the magnetic radiations within the narrow bandwidth of the microwave frequency region (8.2-12.4 Hz) [2]. Gratifyingly, these conductive nanopapers showed a magnetic effectiveness of almost 99 %. This shed light on the suitability of cellulose nanopapers for varied high-end technological applications due to their flexibility, chemical resistance, and superior mechanical properties. However, whether the fabricated films were based on CNCs or CNFs, the colloidal aspect of the suspensions after the aniline polymerization was somehow overlooked and there is a lack of literature regarding this particular issue, despite its relevance for harnessing electromechanical properties of the final films.

Another aspect that is often overlooked is the mode of interaction of PANI during the *in-situ* oxidative polymerization of aniline in the presence of NCs. More specifically, whether the hydroxyl groups on the surface of NCs are chemically involved in the polymerization process by acting as a transfer or initiating site, or just physically interacting with PANI chains has not been

discussed in detail. This aspect is of key importance in controlling the properties of PANI/NC hybrid materials. Indeed, to take advantage of both the attributes of NCs (strength, nanoscale, high-specific surface, colloidal stability in water, reinforcement) and PANI (electrical and dielectric properties) in the hybrid PANI/NC materials, the NCs should act as a nucleating site during the polymerization of PANI for better control of the thickness of polymer and morphology of the PANI/NCs at the nanoscale. To our knowledge, the only article that emphasized the functionality of NCs was published by Fei et al. in which epoxy groups were incorporated into bacterial cellulose (BC) scaffolds by chemical grafting of epoxy chloropropane (ECP) onto BC nanofibrils [35]. Then, PANI was chemically grafted onto the epoxy-modified BC (PANI-*g*-EBC) to improve the interaction and compatibility between PANI and BC, as well as to promote the formation of more uniform and continuous conductive paths.

In comparison with neat NCs, the functionalization of NCs with amino groups further expands the reactivity of NCs toward a wide range of chemical reactions, and impart effective colloidal stability over a broad pH domain from 2 to 12, thanks to the protonation aptitude of NH_2 groups. In addition, the NH_2 function demonstrates a higher aptitude to polymer grafting either through transfer reaction or by acting as an initiator site [36]. Given the harsh conditions during the oxidative polymerization of aniline (at pH 2 and in the presence of a high concentration of KPS), and the necessity to avoid the NC aggregation during the *in-situ* AN polymerization in the presence of NCs, amino-functionalized CNCs were used in the present work, instead of neat CNCs, to prepare hybrid PANI/NCs. The CNCs bearing a NH_2 primary amino function were prepared by periodate oxidation followed by a reaction with ammonia, forming an imine Schiff base that was subsequently reduced to primary amine using $NaBH_4$ in water. The aminated CNCs, referred to as DamCNCs in the following, were hybridized with PANI via conventional oxidative polymerization of aniline with ammonium persulfate in water, giving rise to a stable colloidal dispersion. The colloidal properties of the hybrid PANI/DamCNC systems, their morphology, and electrical conductivity were investigated in details. The mechanism of PANI growth on the surface of DamCNCs was discussed, and the key role of the amino function was highlighted. As potential application of PANI/DamCNCs, conductive nanopapers prepared by mixing PANI/DamCNCs at different contents, with CNFs suspension (either anionic or cationic CNFs) was prepared, and the critical role of the surface charge of CNFs in controlling the properties of the nanopaper was discussed. Although PANI/NCs prepared via *in-situ* polymerization have been the subject of numerous papers, the main novelty of the present work is as follows: (i) The use of aminated CNCs in the preparation of PANI/NCs has not been reported so far, opening the way to a better control of the colloidal stability of

PANI/CNC-based materials, as well as the morphology of the appended PANI. (ii) The grafting mechanism of PANI onto CNCs was discussed and correlated with the functionality of the CNCs. (iii) The use of PANI/CNCs as an additive to prepare flexible conductive and tough nanopaper by wet processing in water has never been reported, providing a sustainable alternative to thin-conductive nanopaper.

2. EXPERIMENTAL SECTION

2.1. Materials

Never-dried eucalyptus pulp (NDP) with a water content of 50 wt% was kindly supplied by Torraspapel S.A. (Spain) and used as starting material for the preparation of both CNCs and CNFs. Sodium meta-periodate ($NaIO_4$), sodium hydroxide (NaOH), hydrochloric acid (HCl, 37 vol%), ammonium acetate ($NH_4CH_3CO_2$), ammonia (NH_3), sodium borohydride ($NaBH_4$), hydroxylamine hydrochloride (NH_2OH_HCl), aniline (≥ 99.0 %), ammonium persulfate (APS) (≥ 98.0 %) were purchased from Sigma-Aldrich and used without further purification. Commercial CNCs were purchased from CelluForce (Canada).

2.1.1. Preparation of diaminated cellulose nanocrystals (DamCNCs)

Colloidal diaminated cellulose nanocrystals were prepared according to the method described by Koshani et al. [37] with minor modifications. In brief, 5.0 g of eucalyptus pulp was dissolved in 300 mL of distilled water, and 6.6 g of $NaIO_4$ was added. The suspension was kept in the dark and under magnetic stirring for 48 h at 40 °C. The recovered suspension was washed 3 times with distilled water and dispersed using a T25 Ultra Turrax homogenizer at 13,500 rpm for 1 min. The resulting dialdehyde cellulose nanocrystals will be referred to as DalCNCs in the following. The aldehyde content was determined by pH titration, after the reaction of the DalCNCs with hydroxylamine hydrochloride, according to the method reported in the literature [37,38].

To proceed with the amination step, the DalCNCs were dewatered through solvent exchange with ethanol for 3 cycles, each one including stirring for 10 h followed by centrifugation for 5 min at 400 rpm. This step was crucial because the remaining water in DalCNCs could interfere in the amination by hydrolyzing ammonia to ammonium and hydroxide [37]. The solvent-exchanged sample was dispersed in 200 mL of ethanol containing a desired amount of $NH_4CH_3CO_2$ (3 mol per mol -CHO group) and NH_3 (10 mol per mol -CHO). The reaction was carried out at 60 °C for 18 h, then cooled down in an ice bath, and 0.46 g of $NaBH_4$ was added dropwise to the suspension under vigorous stirring for 3 h. Finally, the resulting

sample, referred to as DamCNC in the following, was thoroughly washed with distilled water and the amine groups were subsequently dosed. **Scheme 1** summarizes the successive steps of the preparation of DamCNCs. The amine groups of DamCNCs were quantified by conductometric titration with a standardized HCl solution, according to the method detailed in the literature [37]. The amine content was found to be around 2.6 mmol g^{-1} (**Figure S1**).

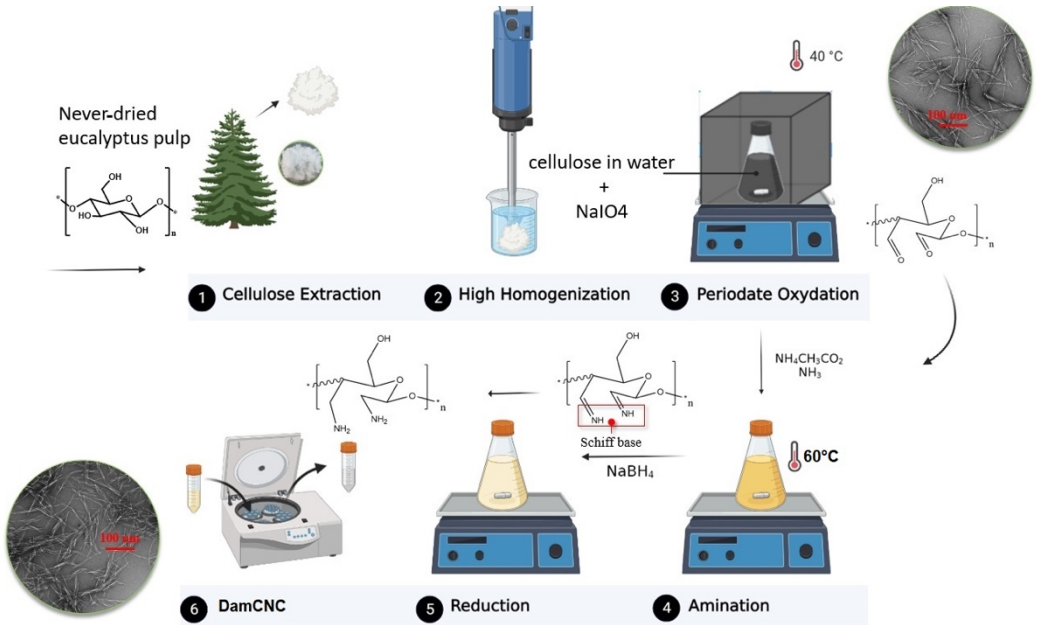

Scheme 1: Preparation steps of diaminated cellulose nanocrystals from never-dried eucalyptus pulp (softwood pulp).

2.1.2. Preparation of colloidal PANI/DamCNC nanohybrids

Aniline was polymerized *in situ* in the presence of DamCNCs as follows: 0.1 g of DamCNC suspension (dry basis) was dispersed in an aqueous 1 M HCl solution for 1 min using ultrasonication (Sonics Vibracel Model CV33) at a 40 % amplitude. Then, 0.6 g of aniline dissolved in 10 mL of 1 M HCl and kept under stirring to ensure the dissolution and protonation of the monomer, was added to the DamCNC suspension. The mixture was then stirred in a temperature-controlled ice bath (0 °C). The APS solution (APS/aniline ratio of 1.33 wt%) was gradually added to the reaction system over 30 min and the polymerization was carried out for 3 h. The color of the suspension turned to dark blue in the first 2 min, then to dark green, and remained the same throughout the reaction. The resulting product was washed several times by centrifugation with distilled water to remove any by-products or remaining reagents. Finally, the pH was adjusted with a few drops of a 1 M HCl solution to guarantee that PANI was in its conductive ES form.

2.1.3. Preparation of cationic and anionic cellulose nanofibrils

The preparation of anionic CNFs (ACNFs) was achieved by the TEMPO-mediated oxidation of cellulose fibers (bleached eucalyptus pulp) following the method previously described by Besbes et al. [39]. Cationic CNFs (CCNFs) were produced by pretreating of cellulosic fibers with glycidyltrimethylammonium chloride (GTMAC) followed by their disintegration by a high-pressure homogenizer (NS1001L PANDA 2 KGEA, Italy) under a pressure between 300 and 600 bar, following the procedure reported in our previous work [40]. The nanofibrillar morphology of the two types of CNFs is illustrated by TEM images in Supplementary **Figure S2**.

2.1.4. Film preparation

CNF films and PANI/DamCNC nanocomposite films were prepared according to the following procedure. The CNF suspension was diluted to 1 wt% solid content and sonicated for 30 s. Previously prepared PANI/DamCNC suspensions with contents of 20, 40, 50, 60, and 80 wt% of the total dry weight of the CNF suspension, were added and gently stirred for 10 min. The mixture was vacuum-filtered until cakes were formed on the surface of a membrane filter (pore size 0.45 µm). Films were kept at 23 °C and 50 % relative humidity. The prepared nanocomposite films were compared to a reference film made of pure CNFs. The overall procedure of the film preparation is illustrated in **Scheme 2**.

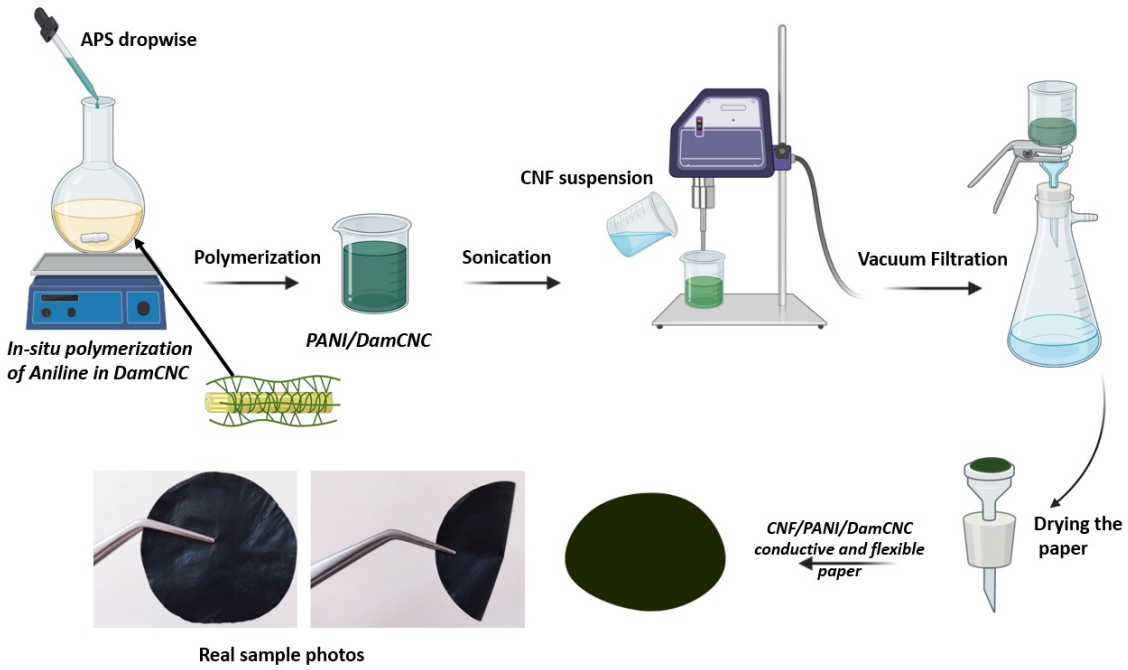

Scheme 2: Schematic illustration of CNF-PANI/DamCNC nanocomposite films by pressure-assisted filtration.

2.2. Characterization

2.2.1. Particle size and ζ-potential analysis

The suspensions were diluted either with distilled water or ethanol. The size distribution and ζ-potential of all the dispersions were characterized using a Zetasizer ZS analyzer (Malvern Ltd, U.K) at a concentration of ca. 0.02 wt%. The pH was varied from 2 to 10. Each sample was analyzed in triplicates and the resulting values were averaged to determine the mean particle size and ζ-potential. The polydispersity index (PDI) which is dimensionless and measures the broadness of the size distribution calculated from the cumulant analysis, was assessed as well.

2.2.2. Transmission electron microscopy (TEM)

Dilute aqueous dispersions of DamCNCs, PANI/CNCs and PANI/DamCNC nanohybrids were sonicated for 30 s, then deposited on carbon films supported by copper TEM grids. After 2 min, the liquid in excess was blotted with filter paper and, before drying, a droplet of 2 wt % uranyl acetate negative stain was deposited on the specimens. The stain in excess was blotted and the remaining liquid film allowed to dry. The specimens were observed with a JEOL JEM 2100-Plus microscope operating at a voltage of 200 kV. The images were recorded with a Gatan Rio 16 digital camera.

2.2.3. Scanning electron microscopy (SEM)

Film fragments were fixed on metallic stubs with carbon tape and sputter-coated with Au/Pd. Their surface was observed in secondary electron mode with a Thermo Scientific FEI Quanta 250 microscope equipped with a field-emission gun (FEG) and operating at 2.5 kV.

2.2.4. X-ray diffraction (XRD)

Pure PANI, DamCNC and PANI/DamCNC powders were poured into 1-mm glass capillaries that were flame-sealed and X-rayed in vacuum using a Philips PW3830 generator operating at 30 kV and 20 mA (Ni-filtered CuKα radiation, λ = 0.1542 nm), during 1.5-h exposures. Two-dimensional diffraction patterns were recorded on Fujifilm imaging plates, read offline with a Fujifilm BAS 1800-II bioimaging analyzer. Diffraction profiles were calculated by rotationally averaging the 2D patterns.

2.2.5. ^{13}C CP/MAS NMR spectroscopy

^{13}C CP/MAS NMR spectroscopy was performed using a Bruker Avance DSX 400 MHz spectrometer operating at 100.6 MHz under a cross-polarization, high-power proton decoupling and magic angle spinning (CP/MAS) at a 12 kHz spinning speed, a sweep width of 29761 Hz, and a recycle delay at 2 s. Each spectrum was averaged over 6000 scans. The ^{13}C chemical shifts were calibrated with the resonance of the glycine carboxyl group at 176.03 ppm.

2.2.6. Vibrational spectroscopies

Fourier-transform infrared (FTIR) spectroscopy was carried out on a Perkin Elmer spectrometer in the 4000−400 cm^{-1}. Raman spectra were recorded on a LabRAM analytical Raman using a He−Ne laser source as the exciting radiation (λ = 633 nm) and an air-cooled CDD detector. The acquisition time was 100 s. In both FTIR and Raman spectroscopies, a thin film of dried sample was used.

2.2.7. Thermal stability

The thermal stability of all samples was determined by thermogravimetric analysis (TGA) using a TGA 400 thermogravimetric analyzer from Perkin Elmer under an airflow in the temperature range of 50−800 °C at the heating rate of 10 °C min^{-1}.

2.2.8. Electrochemical and supercapacitors characterization

Electrochemical measurements by cyclic voltammetry were performed with a DropSens μStat 400 Potentiostat operated by the Dropview 8400 data acquisition software. To evaluate the electrochemical performance of PANI, and PANI/DamCNC prepared composites, cyclic voltammetry (CV) curves were obtained in the potential range from 0 to 0.8 V by varying the scan rate (10, 20, 50, and 100 mV) in 1 M H_2SO_4 electrolyte. Screen-printed carbon electrodes (SPCEs) were purchased from Metrohm Dropsens (Tunisia). The platform used was DRP-C110, constituted of a 4-mm diameter carbon working electrode, a silver pseudo-reference electrode, and a carbon auxiliary electrode. To modify the bare SPCE, 20 μL of PANI, DamCNCs, and PANI/DamCNCs was directly drop-cast onto the surface of the working electrode and left to dry at room temperature until further use.

The electrochemical performance of the CCNF-PANI/DamCNC nanocomposite as supercapacitors was evaluated using CV, galvanostatic charge-discharge (GCD), and electrochemical impedance spectroscopy (EIS) analysis, and it was compared to pristine CCNF and PANI/DamCNC modified electrodes. All electrochemical measurements of the electrodes were conducted at 25 °C using a three-electrode system (Ag/AgCl reference electrode, a stainless-steel auxiliary electrode, and a coated stainless steel working electrode) in which the specific capacitance of the nanopaper using CCNFs prepared with 50 wt% PANI/DamCNCs was assessed using cyclic voltammetry analysis. The specific capacitance (C_{sp}) was deduced from the cyclic voltammograms using **Eq. 1**:

$$C_{sp} = \frac{\int I\, dV}{m \times v \times \Delta V} \qquad \textbf{(1)}$$

where I is the current intensity (A), m is the mass of the electroactive material (g), v is the scan rate (V/s) and ΔV is the potential window of the cyclic voltammogram (V).

The galvanostatic charge–discharge (GCD) experiments were carried out over the potential range of -0.2 to 0.8 V. Electrochemical impedance spectroscopy (EIS) was carried out between 0.01 Hz and 0.1 MHz at the open circuit potential.

2.2.9. Conductivity measurements

The electric conductivity of all samples was measured using a Novocontrol Broadband dielectric spectrometer, based on an α analyzer and a Quatro temperature controller. Dielectric conductivity data were recorded using the Win DETA impedance analysis software.

3. RESULTS AND DISCUSSION

3.1. FTIR and Raman spectroscopies

The evolution of the chemical structure following the $NaIO_4$ oxidation, amination, and PANI grafting was studied by FTIR, Raman, and NMR spectroscopies. In the FTIR spectra given in **Figure 1A**, the emergence of the typical CO band around 1730 cm^{-1} in DalCNCs confirmed the occurrence of the oxidation to generate aldehyde groups [41]. The disappearance of this band and the appearance of a new band around 1570 cm^{-1}, assigned to C-N bending vibration in C-NH_2, corroborate the conversion of the aldehyde to amino groups [37]. Apart from these new bands, no evolution in the FTIR spectra could be seen after periodate oxidation and amination with NH_3, which further supports that under the selected conditions, the occurrence of chemical reactions was essentially limited to the surface of cellulose nanocrystals, preserving the core structure of the nanocellulose. The amine content of DamCNCs assessed by conductimetric titration was estimated to 2.6 mmol (**Figure S1**), which is relatively high and suggests a high surface density of NH_2 groups on the surface of DamCNCs.

After the polymerization of aniline in the presence of DamCNCs, a substantial evolution in the FTIR spectra could be seen, with a magnitude that depended on the ANI/DamCNC ratio before polymerization. At a 6/1 ANI/DamCNC ratio, the spectrum was mainly dominated by the PANI bands, while at a 1/1 ratio, those of cellulose dominated the spectrum, as shown in **Figure 1B** [42]. For the former, the spectrum shows the typical bands of PANI at 1180 cm^{-1} associated with the vibration mode of the –NH+=, 1240 cm^{-1} (C–N^+ -stretching vibration in the polaron structure), 1350 cm^{-1} (C-N stretching vibration=), 1500 cm^{-1} (benzenoid ring of the polymer chain), and 1620 cm^{-1} (quinoid stretching vibration) [42,43]. At a 1/1 ANI/DamCNC ratio, the bands from PANI were only visible as shoulders overlapping with the bands of cellulose. In comparison with the quinoid vibration of pure PANI occurring at 1620 cm^{-1}, the shift of the corresponding band from PANI/DamCNCs was presumably due to the strong interaction between the quinoid ring of PANI and the DamCNCs (**Figure 1C**) [44].

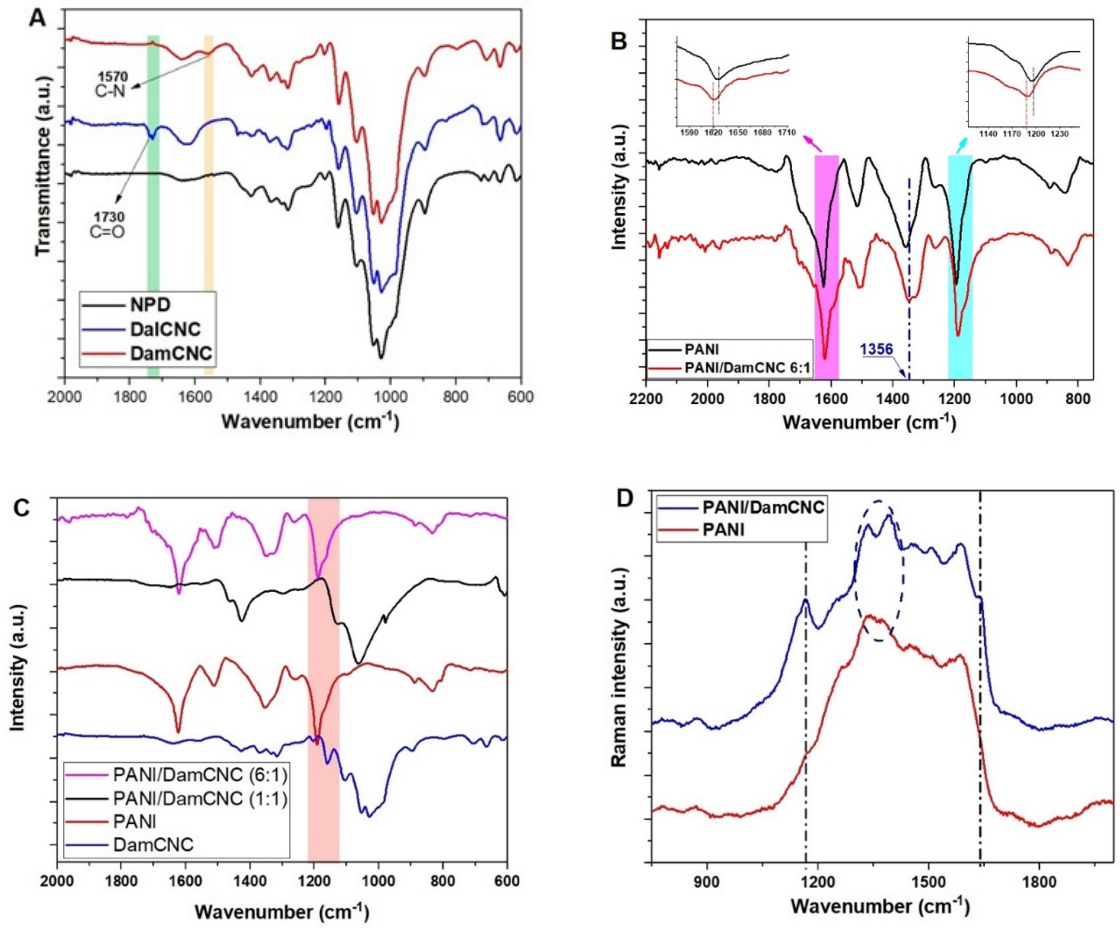

Figure 1. (A-C) FTIR spectra of neat cellulose, DalCNCs, DamCNCs and PANI/DamCNCs; (D) Raman spectra of pristine PANI and PANI/DamCNC nanohybrids.

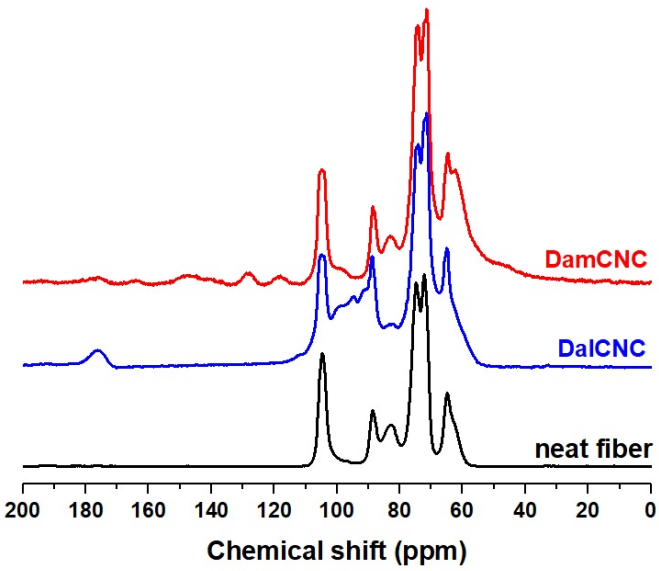

Figure 2: ^{13}C CP/MAS NMR spectra of NDP cellulose fibers, DalCNCs and DamCNCs. (aldehyde content = 3.4 mmol g^{-1}, amine content = 2.6 mmol g^{-1}).

As observed in **Figure 1D**, the normalized Raman spectra of the PANI/DamCNC nanocomposite presented typical bands, especially around 1250–1330 cm^{-1}, which were attributed to the amine bands assigned to DamCNC and indicate that a considerable amount of N-H has been attached to PANI chains. In addition, a small shift of the peak of C=C quinoid vibration to 1630 cm^{-1} was noted. This indicated a strong interaction between the quinoid ring of PANI and the DamCNCs, revealing a high coverage of DamCNCs by PANI [45].

3.2. ^{13}C CP/MAS NMR spectroscopy

The CP/MAS spectra of NDP cellulose, DalCNCs, and DamCNCs were recorded to further highlight the structural change following the different chemical treatments of cellulose (**Figure 2**). The spectrum of neat cellulose displayed the typical peaks of cellulose I associated with the chemical shifts of the carbon atoms in the AGU [46]. At 60-70 ppm, the two peaks correspond to C6, with the first one around 62 ppm relative to the contribution from the surface (disordered region), and the second at 65 ppm related to the crystalline core. The peaks between 70 and 80 ppm were assigned to carbons C2, C3 and C5 of the AGU. The two peaks at 83 and 88 ppm were attributed to the C4 carbons of disordered cellulose including the surface chains and to the crystalline core, respectively. The peak at 105 ppm was attributed to C1 carbons.

After the oxidation reaction, the main evolution in the NMR spectrum of DalCNCs was the emergence of a broad signal between 90-100 ppm that was assigned to the hemiacetal function resulting from the recombination of part of aldehyde groups with neighboring hydroxyl groups [47]. The emergence of this broad signal was reported in the literature, mostly when the degree of oxidation exceeded 0.3 [48]. A broad peak at 175 ppm was observed in the DalCNC spectrum, typical of the CO groups of aldehydes, indicating that a fraction of aldehyde groups remained free and not combined with neighboring hydroxyl groups into hemiacetals. This result disagrees with literature data, where no CO signal could be seen in ^{13}C solid-state NMR. However, the appearance of the CO signal in the DalCNC spectrum agreed with FTIR data that showed the presence of the CO band at 1730 cm^{-1}. After the amination with NH_3, and subsequent reduction by $NaBH_4$, the broad hemiacetal signal in the 90−100 ppm region almost disappeared as well as the CO signal at 175 ppm. This indicated that all of the aldehyde groups were consumed by the amine, and most of the hemiacetal groups were also readily converted into amine during the reductive amination process. Two weak signals at 130 and 120 ppm emerged after the reductive amination by NH_4OH, which might be assigned to C=C groups stemming from the β-elimination reaction likely to occur in the presence of a base [49,50]. Unfortunately, the NMR spectrum of PANI/CNCs could not be recorded due to the high shielding properties of PANI.

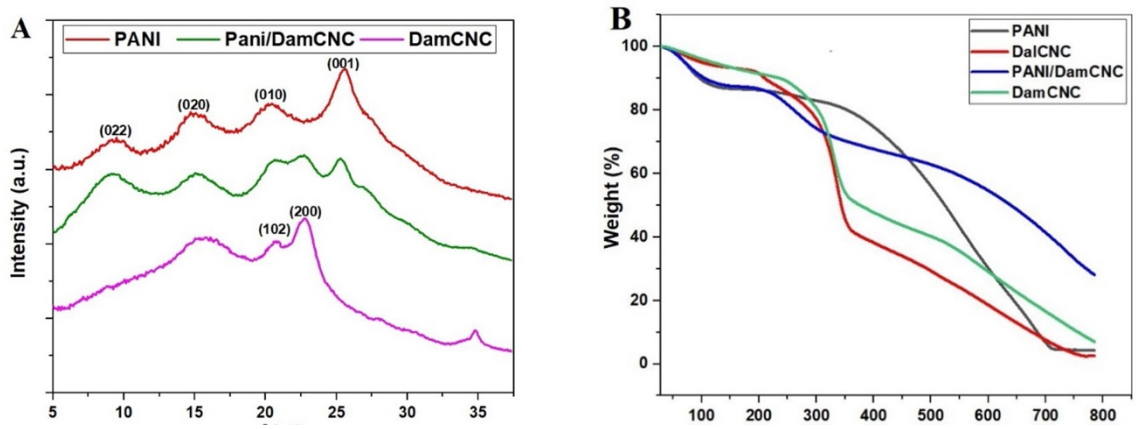

Figure 3: (A) XRD profiles of pristine PANI, DamCNCs and PANI/DamCNC nanohybrids; (B) TGA curves of PANI, DalCNCs, DamCNCs and PANI/DamCNC nanohybrids (ANI/DamCNC = 6/1).

3.3. X-ray diffraction (XRD), thermal analysis, and UV-vis spectroscopy

The XRD profile of DamCNCs was similar to that of cellulose I (**Figure 3A**), with peaks at 2θ = 15.2, 16.5, 20.7, 22.7, and 34.9° corresponding to the (110), (1$\bar{1}$0), (102), (200) and (004) crystallographic planes, respectively [38,51]. The profile of PANI contained four broad peaks at around 9.1, 14.9, 20.5, and 25.2°, corresponding to the (022), (020), (010), and (001) crystal planes of PANI in its ES form [2]. As expected, the profile of the PANI/DamCNC film was a combination of the profiles of PANI and DamCNCs.

Figure 3B shows the TGA curves of PANI, DalCNCs, DamCNCs, and PANI/DamCNC nanohybrids recorded under air atmosphere. TGA curves for DalCNCs and DamCNCs showed three weight loss stages. The first stage was about 10 % owing to the evaporation of adsorbed water the second stage begins at 300 up to 400 °C with a weight loss of around 50 % due to the degradation of the saccharide backbone of CNCs. The third and last step occurred up to 400 °C with a *ca.* 30 % weight loss owing to the decomposition of the residual carbon. The onset of thermal degradation of DalCNCs was observed around 200 °C, lower than that of DamCNC with an onset at about 235 °C. This difference in thermal stability was due to the presence of aldehyde groups in DalCNCs that reduced the thermal stability of the cellulose material. The thermogram of pure PANI showed a two-step weight loss, the first occurring between 100 and 300 °C due to the loss of bound water and HCl, and the second occurring between 400 and 800 °C due to thermal degradation of the PANI skeleton. The thermogram of PANI/DamCNCs is a hybrid of DamCNCs and PANI, with a three-stage weight loss beginning with water evaporation at 100-120 °C, followed by a second loss at 200-400 °C, and a last stage observed up to 400 °C involving organic material carbonization.

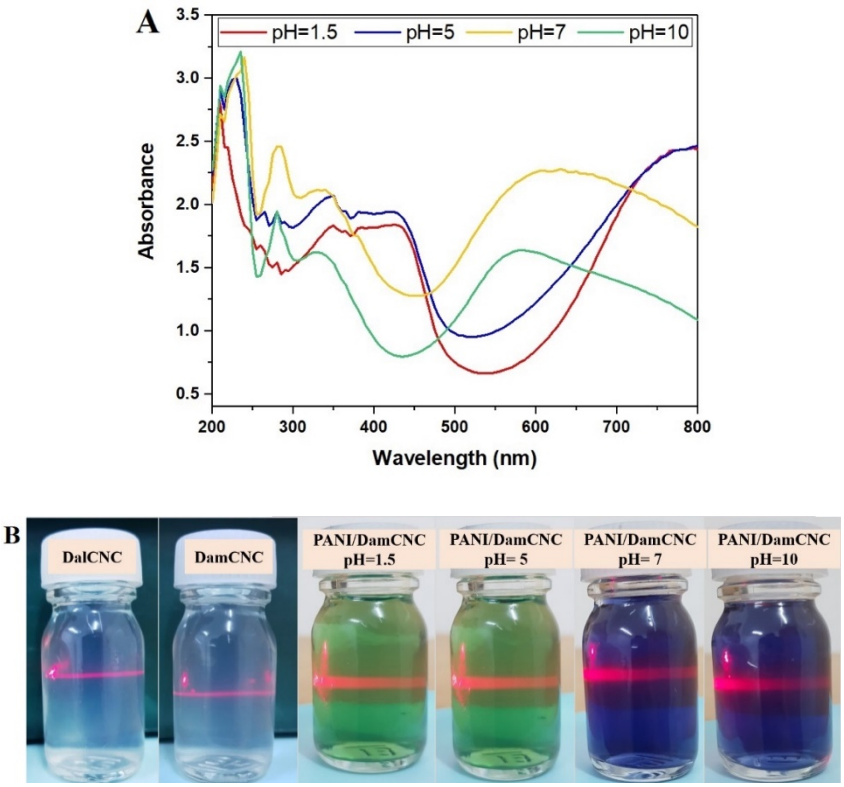

Figure 4: (A) UV-vis spectra of PANI/DamCNC nanohybrid dispersions at different pH values; (B) Visual aspect of the DalCNC, DamCNC, and PANI/DamCNC suspensions at different pH. The red laser beam is visible through the samples.

Figure 4A presents the UV-Vis absorption spectrum of the PANI/DamCNC and PANI/DalCNC dispersions at a 6/1 mass ratio in different pH media. First, PANI seemed to have retained its band structure through the presence of its characteristic peaks while being formed *in situ* onto the DamCNC surface. Second, the electronic state of PANI, in its ES (conducting) or emeraldine-base (EB, insulating) form could easily be identified by analyzing the data from our UV spectra. At low pH values, the nanohybrids exhibited two distinct peaks located at about 410 and 800 nm attributed to the π-π* transitions in benzenoid structure of the aromatic ring and n-π* transitions of the quinoid ring, respectively [52]. This attribution indicates the doped state of PANI corresponds to its ES form. Above pH 7, a visible change in the characteristic peaks was observed through a shift at a lower wavelength of the first transition band to 315-320 nm corresponding to π-π* transitions while a new broad peak at 590-620 nm appeared. This observation strongly indicated the change in the electronic state of PANI from the ES to the EB form [53]. The evolution of the UV-Vis spectra of PANI/DalCNCs was accompanied by a change in the color of the suspension from green to dark blue when PANI changed from the ES to the EB form (**Figure 4B**).

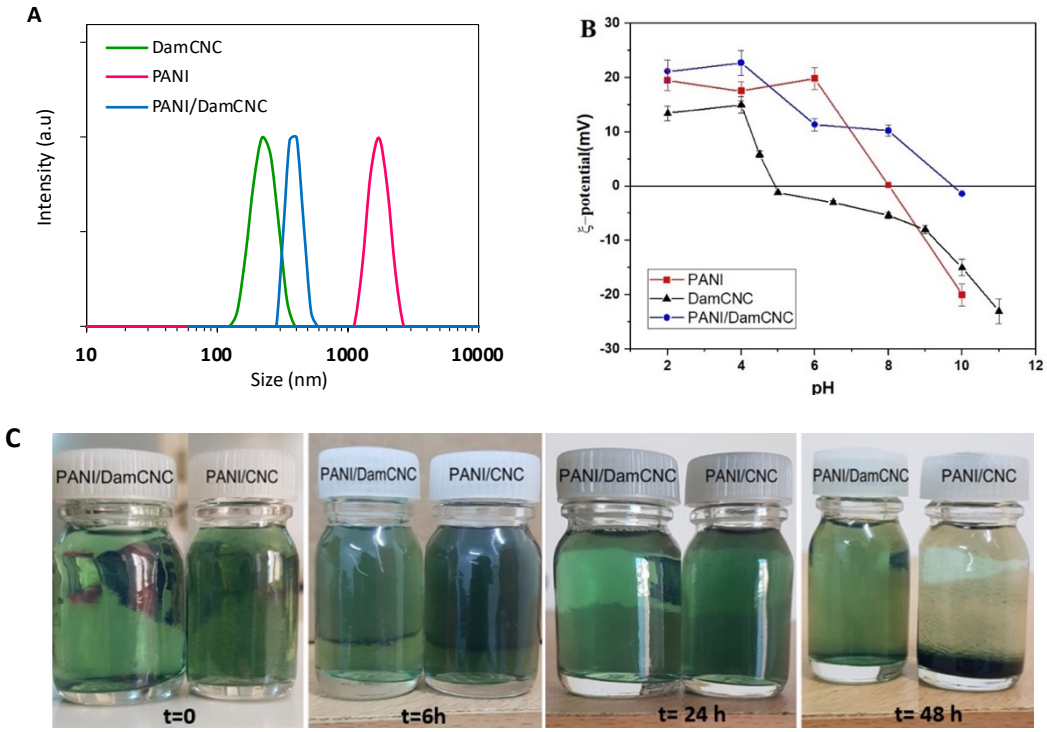

Figure 5: (A) DLS, (B) ζ-potential of the dispersions within different pH range (2-10), and (C) visual aspect of PANI/DamCNC, and PANI/CNC nanohybrid suspensions, at pH 4-5 as a function of resting time.

3.4. Colloidal stability and morphology of DalCNCs, DamCNCs, PANI/DalCNCs and PANI/DamCNCs

To evaluate the potential use of hybrid PANI/DamCNCs as a conductive coating or an additive to polymer latex to produce conductive nanocomposite films, the PANI/NC suspension must be stable against aggregation and should easily be redispersed once the particles settle down. The colloidal properties of DamCNCs and PANI/DamCNCs were studied by DLS and ζ-potential measurements. The particle size distribution of PANI/DamCNCs and neat DamCNCs at pH 3-4, and the evolution of the ζ-potential at different pH are shown in **Figure 5A** and **5B**. DamCNCs showed a monomodal size distribution with a mean value around 300 nm, confirming the nanosize of the particles. After polymerization of aniline, a shift to a higher size was noted in PANI/DamCNCs, with a distribution ranging from 300 to 600 nm. The PANI particles prepared without DamCNC under the same conditions were much larger with a distribution within the range of 1 to 3 µm. The ζ-potential of DamCNCs was positive around +14 mV in the pH domain from 2-4, got close to 0 mV from pH 5 to 6, and became negative over pH 9. This evolution in the ζ-potential was due to the presence of amino groups on the surface of DamCNCs that protonate at pH < 4, and became neutral until the solution was strongly basic. The hybrid PANI/DamCNCs displayed a positive ζ-potential between +20 to +10 mV within the 2-8 pH

range, indicating a positively charged surface within this pH domain. These positive charges originated from the protonation of NH- groups in PANI. The same trend was noted for PANI, which agrees with the literature data.

The colloidal stability was qualitatively evaluated over time by monitoring the visual aspect of the suspension for 48 h. The suspension was first sonicated for 20 s to ensure the fragmentation and redispersion of aggregates likely to be formed during long-time storage of the suspension. The PANI/DamCNC dispersion remained stable over 48 h without any sign of particle sedimentation, unlike the PANI/CNC suspension prepared in the same way as the PANI/DamCNC one (**Figure 5C**). However, using commercial CNCs, the sample settled down within this timescale, with a disappearance of the green color. This indicated a poor colloidal stability of PANI/CNCs in comparison with the PANI/DamCNCs. In addition, the PANI/CNCs were very aggregated after the polymerization reaction, and longer times of sonication were required to maintain some stability. The difference in colloidal stability was explained by the difference in particle size distribution and surface charge. The smaller the particles, and the higher the absolute value of the ζ-potential, the better the colloidal stability. The huge difference in the stability between PANI/DamCNCs and PANI/CNCs demonstrated the importance of the surface functionalization of CNCs in promoting the colloidal stability of the hybrid PANI/nanocellulose suspension.

The periodate oxidation of NDP fibers resulted in rodlike particles with a length of 100-130 nm. The width ranged between 5 and 12 nm depending on the degree of separation of individual crystallites (**Figure 6A**). This morphology agrees with previous works that showed that bleached fibers could easily be fragmented into nanosize particles by mild ultrasonication during a short time after periodate oxidation over a critical level [54]. After the amination reaction with NH_3, no significant change in morphology was observed for DalCNCs, except that the crystallites formed slightly wider bundles (**Figure 6B**).

As seen in **Figure S3**, without the presence of CNCs, aniline polymerized in the form of nodular PANI aggregates, often exceeding a few micrometers in size, hence generally too large/thick for a proper visualization by TEM. The polymerization of aniline in the presence of commercial CNCs also resulted in bulky aggregates. Images could only be recorded from the smallest aggregates in which 200-400 nm-long and about 100 nm-wide rodlike cylinders (**Figure 6C** and **6D**), presumably corresponding to PANI, were observed as well as a significant fraction of ungrafted and bundled CNCs (**Figure 6E**). When DamCNCs were used as substrate for polymerization, two types of PANI particles were observed. On the one hand, images showed cylinders similar to those detected in the PANI/CNC sample (**Figure 6F**). Considering their size

and shape, we assumed that they corresponded to bundles of CNCs that were encapsulated by PANI. However, since only the surface of the cylinders was visible, it was difficult to be sure that they contained CNCs. On the other hand, spiky particles had nucleated and grown from CNCs (**Figure 6G**). They were constituted of rhombohedral crystals that grew radially from the CNC surface, forming star-like particles (**Figure 6H** and **6I**). In our images, this latter form was largely dominant. Still, since the bulkier aggregates could not be observed, it was not possible to quantitatively assess the relative fractions of each form. Complementary TEM images of preparations of PANI/DamCNCs are shown in **Figures S4** and **S5**. In the images of unstained specimens (**Figure S5**), the resolution was limited by the radiation sensitivity of both cellulose and PANI particles. However, the images illustrate the fact that the establishment of a percolating network of PANI particles grown onto the CNCs might be achieved.

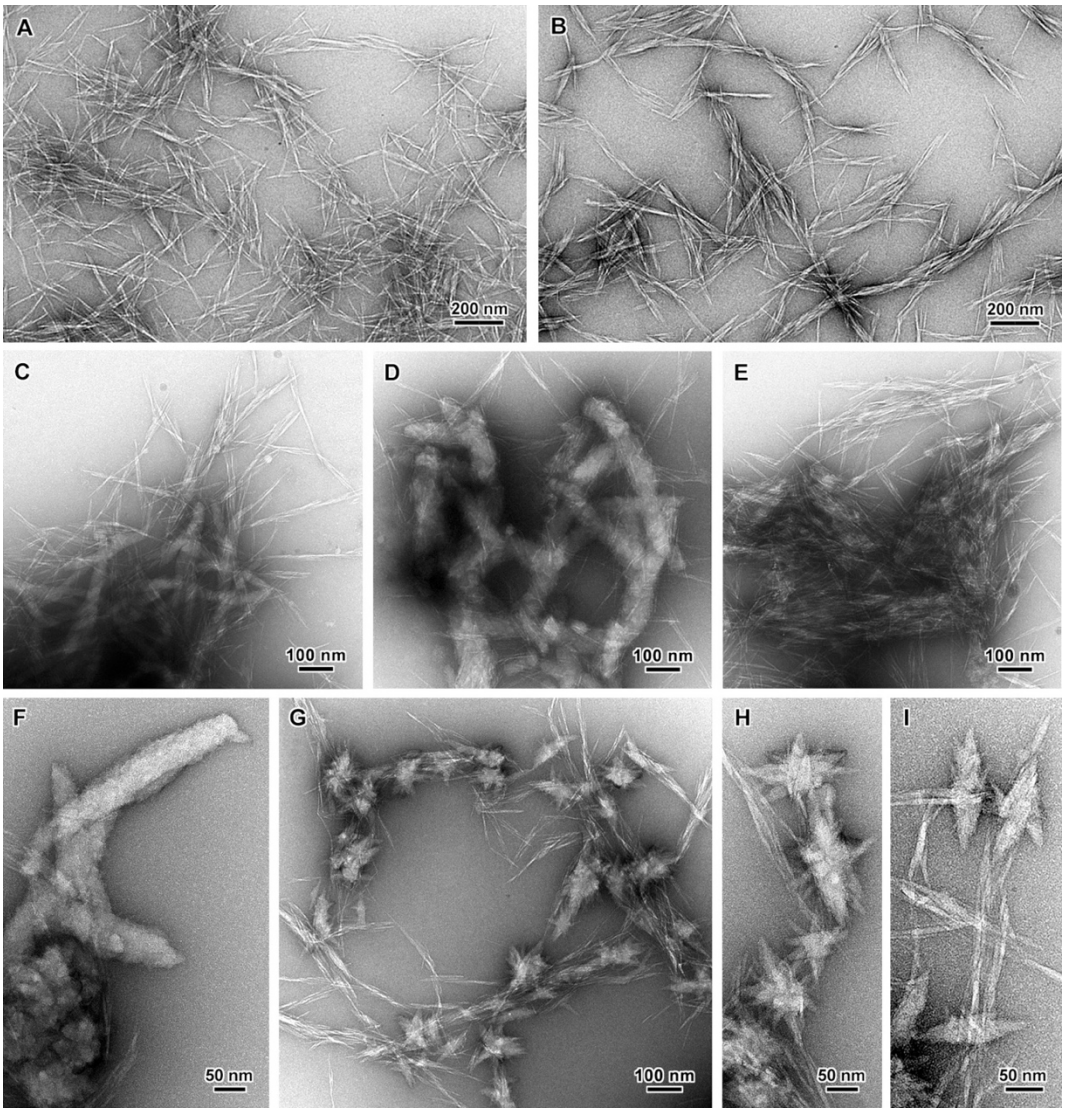

Figure 6: TEM micrographs of negatively stained preparations from DamCNC (A), DamCNC (B), PANI/CNC (C-E) and PANI/DamCNC (ANI/DamCNC = 6/1) (F-I) suspensions.

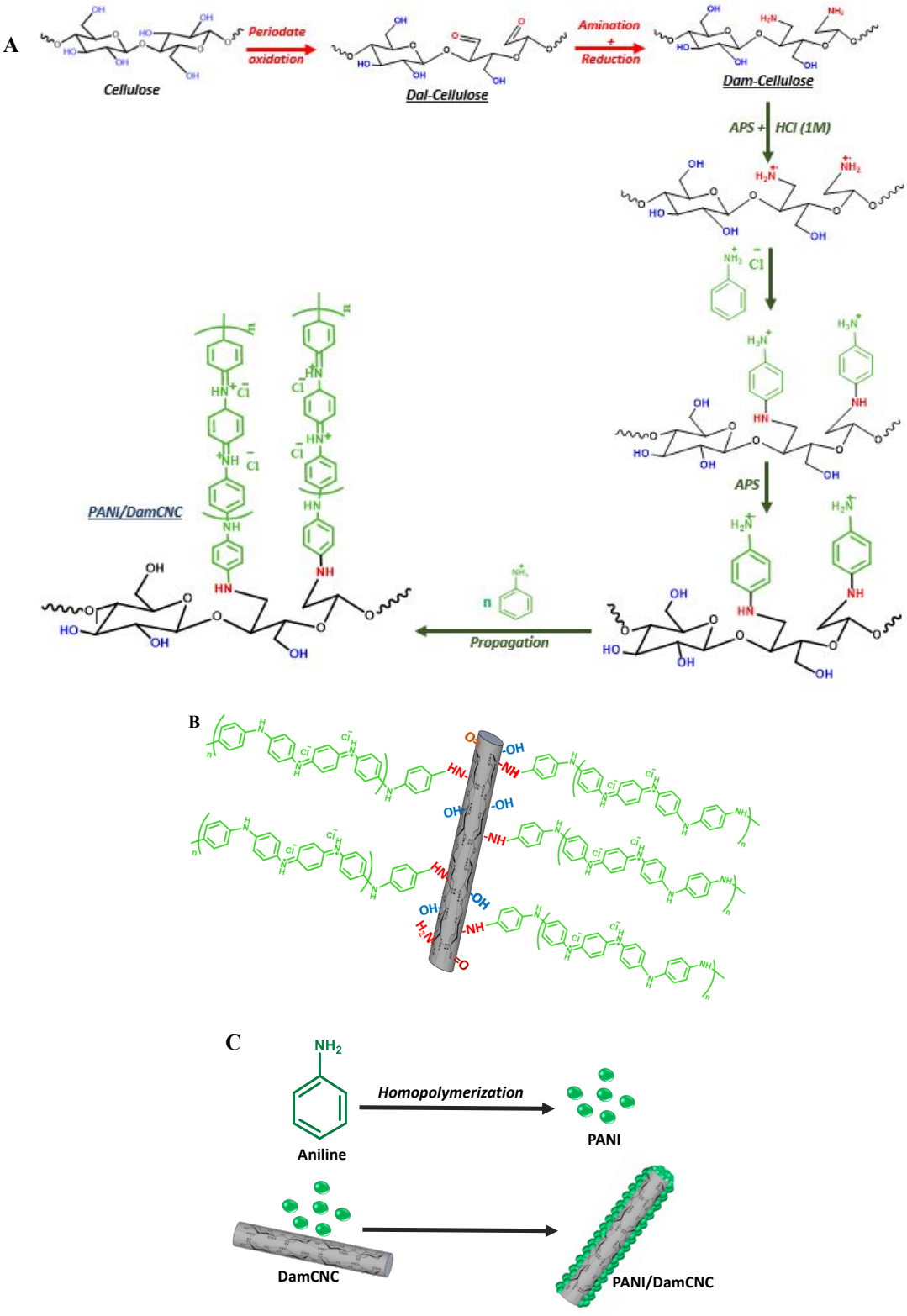

Figure 7: Synthesis mechanism of PANI/DamCNC (only one surface chain was presented for clarity) (A) Schematic model illustrating the assembling of PANI at the surface of DamCNCs resulting in a star-like morphology (B), and a cylindrical-shape (C).

3.5 Mechanism of formation of PANI in DamCNCs and CNCs

Based on the above characteristics of the PANI/DamCNCs, the following mechanism was proposed for the growth of PANI onto DamCNCs (**Figure 7**). At pH 2, the amino groups of DamCNCs were protonated in the form of NH_2^+. The NH_2^+ was readily oxidized by persulfate into $NH_2^{+\cdot}$ which initiated the polymerization and the grafting of PANI on the surface of DamCNCs. The growth of PANI occurred by the reaction of the growing oligomer radical cations with aniline radical cations until depletion of aniline. The preferential growth of PANI on the surface of DamCNCs to the detriment of homopolymerization in solution was likely due to the higher initiation rate from the $-NH_2^{+\cdot}$ compared to the aniline radical cation and to the high density of surface NH_2 groups on DamCNCs. The higher reactivity of $-NH_2^{+\cdot}$ toward the aniline radical cation is explained by the difference in the electronic structure of the two species: in the former, the radical is localized, while in the later the radical is stabilized by delocalization on the benzene ring. Since PANI grew radially from the surface of DamCNCs, and a high density of NH_2 groups is available on the surface of DamCNCs, this reaction pathway resulted in the star-like morphology observed in **Figure 6G** to **6I**, which was the dominant morphology. However, in addition to the star-like morphology, some of PANI/DamCNCs displaying a cylindrical-shape morphology (**Figure 6F**). We imputed this morphology to the coating of DamCNCs by PANI particles generated through the homogeneous polymerization of aniline in the suspension. The formed PANI NPs were deposited/aggregated on the surface of DamCNCs by hydrogen interaction with the surface NH_2 groups of DamCNCs. However, a fraction of DamCNCs appears to be devoid of any PANI, meaning that no PANI was grown or deposited on the CNCs. A possible reason is that more aniline is needed to ensure the full coating of the DamCNC with PANI. Work is under progress to further understand this discrepancy and investigate its effect on the electrical performance of PANI/DamCNCs.

It is worth mentioning, that a different morphology was observed when CNCs prepared from the H_2SO_4 hydrolysis route were used instead of DamCNC, and under similar aniline polymerization conditions. In this case, most of the CNCs were aggregated, with sporadic cylindrical shape morphology (about 50 nm in diameter). This clearly highlights the key role of the amino function in controlling the morphology of the PANI/CNCs and affect their colloidal and electrical properties.

3.6. Electrochemical characterization: cyclic voltammetry of PANI/DamCNC nanocomposite films

Figure 8A showed the CV curves of pristine DamCNCs, pristine PANI and the composite PANI/DamCNCs within the potential range from 0 to +0.8 V in 1 M H_2SO_4 at a scan rate of 20 mV s^{-1}. It is worth mentioning that the redox process is absent in the DamCNCs, and the CV

curves showed a very weak current, resulting in a poor electrochemical response. This suggests that cellulose nanocrystals had a minor effect on the specific capacitance. By contrast, the shape of the CV curve of pure PANI was quasi-rectangular, revealing the strong pseudo-capacitance behavior of PANI that contains two pairs of redox peaks A/A_1 and B/B1, indicating the occurrence of two electrochemical reactions. These redox reactions are reversible and can be attributed to the insertion and removal of protons and electrons from the PANI polymer chain. The first A/A1 peaks, at a potential of around 0.25 V, were attributed to the redox transition of PANI between a semiconductive leucoemeraldine form to a conductive polaronic ES form, while the B/B1 peaks (at a potential of around 0.55 V) corresponded to the emeraldine-to-pernigraniline transition [55].

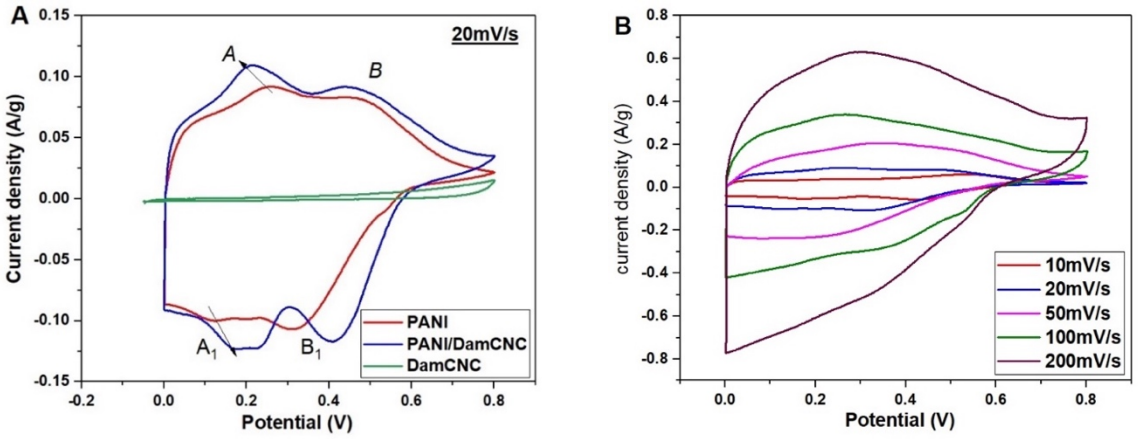

Figure 8: (A) CV curves of PANI, DamCNCs and PANI/DamCNC-modified electrode at 20 mV s^{-1}; (B) CV curves of PANI/DamCNC-modified electrode at different scan rates in 1 M H_2SO_4.

For PANI-grafted DamCNCs, the CV trace exhibited an enhanced electrical response when compared to those of PANI and DamCNCs individually (**Figure 8A)**, suggesting a synergistic effect of the association of DamCNC with PANI as conducting fillers [29]. The nanoscale architecture of PANI/DamCNC nanocomposites with interlaced network structures significantly improved the interface regions between the electrode and the electrolyte, allowing electrolyte ions to diffuse more easily. As a result, more conductive pathways were generated, resulting in a faster electrolyte ion movement during charge/discharge operations and improved electroactive behavior of the PANI/DamCNC nanocomposites. Meanwhile, the redox current density of this sample becomes larger as the scan rate increased (**Figure 8B**), meaning that a better distribution of PANI/DamCNCs resulted in the formation of a conductive network with a higher specific capacitance (deduced from the area of closed CV which was much larger than that of pure PANI), and electrical conductivity.

3.7. PANI/DamCNCs as additives for conductive nanopapers

One of the objectives of our study was to produce thin conductive nanopapers via wet chemistry by adding PANI/DamCNCs to a CNF suspension in water without any organic solvent nor chemical dopant, aiming at imparting flexibility and toughness to the composite nanopaper. The PANI/DamCNCs were meant to impart conductivity while the CNFs conferred mechanical strength and stiffness through their aptitude to set up an entangled network stabilized by hydrogen bonding. Thanks to the nanoscale of CNFs, their fibrillar character, and the presence of a high density of surface hydroxyl groups, a thin film with a high toughness exceeding those of thin polymer films with a thickness at the micron scale was obtained by casting, blade-coating or filtration through microporous membranes, followed by drying. It is worth mentioning that films prepared from PANI/DamCNC suspension only were extremely fragile and did not withstand any deformation, as shown in **Figures 9** and **S6,** hence the necessity of mixing PANI/DamCNCs with CNFs.

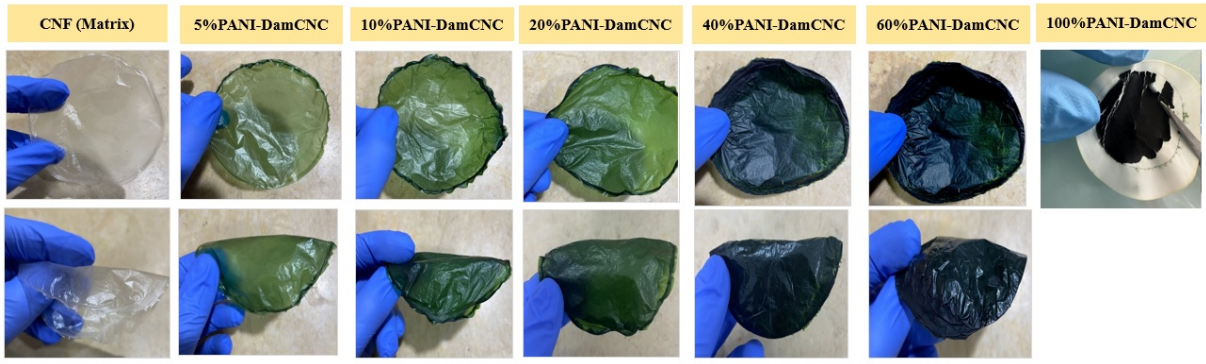

Figure 9: Photographs of CCNF films with different loadings of PANI/DamCNCs.

Two types of CNFs differing by their surface charge, were tested, and both were prepared via chemical pretreatment, including either TEMPO-mediated oxidation or cationization, followed by high-pressure homogenization [40]. The difference in surface charges of the two CNFs was confirmed by ζ-potential measurement (**Figure 10B**). Different amounts of PANI/DamCNCs were added to the CNF suspensions, and after mechanical mixing, a thin film was prepared by vacuum filtration through a microporous PVDF membrane. For all samples, containing CNFs, self-standing films were obtained. These films were highly flexible, resistant, and exhibited increasing green color intensity with increasing PANI/DamCNC content. Without CNFs, PANI/DamCNCs formed a friable fragile film, lacking cohesion. This effect was presumably due to the rodlike morphology of the pristine CNCs. Indeed, CNCs are rigid and stiff so the set-up of an entangled network of CNCs after the removal of water and the formation of

the thin CNC film was unlikely. This explains why CNC-based nanopapers are extremely fragile and stiff. The impact of the stiffness of PANI/DamCNCs became even more pronounced after the grafting of PANI owing to the T_g for PANI (exceeding 100 °C) [56].

The colloidal properties of the CNF and PANI/DamCNCs mixture markedly differed according to the surface charges of the CNFs. Indeed, as shown in **Figure 10A**, ACNFs immediately flocculated upon adding PANI/DamCNCs, irrespective of the CNF-PANI/DamCNC ratio, while in the presence of the CCNFs, the suspension remained colloidally stable over several hours at rest. The instant flocculation of ACNFs resulted from two phenomena. On the one hand, at a pH below 3, the protonation of the carboxyl groups of the ACNFs made the CNF surface neutral while, on the other hand, the positive surface charge of PANI interacted with the carboxyl groups of CNFs via electrostatic interaction, resulting in the neutralization of the surface charge of CNFs and aggregation in the ACNF-PANI/DamCNC mixture. For CCNFs, the fibrils remained positively charged over the whole pH domain from 2 to 12, thanks to the presence of ammonium groups, and preventing possible interaction between the PANI/DamCNCs and CCNFs, leaving the suspension colloidally stable (**Figure 11C**) [40]. This ensured the homogeneous distribution of the PANI/DamCNC particles within the CCNF network that acted as a mechanically stable scaffold. It is worth mentioning that transparent films and self-standing thin nanopapers were obtained by casting CCNF-PANI/DamCNC mixtures in a Teflon mold and drying at 40 °C for several hours.

3.8. Electrical conductivity of CNF-PANI/DamCNC nanopapers

To investigate the electrical properties of the different films, the electrical conductivity of CCNF and ACNF nanocomposites with varying contents in PANI/DamCNCs was measured and the results are shown in **Figure 11**. The electrical conductivity of polymer nanocomposites is known to depend on the composition of the materials and the dispersion or distribution of the conductive particles within the polymer matrix. Neat CNF nanopapers are insulating by nature having a conductivity between 10^{-8} and 10^{-5} S m^{-1}. The conductivity of ACNF nanopaper remained below 10^{-3} S m^{-1}, even for high content in PANI/DamCNCs. Agglomeration and flocculation inhibited the formation of a conductive route along the grafted PANI, which might explain the low conductivity of ACNF-PANI/DamCNC films and their insulating character. In contrast, when mixed with CCNFs, a significant increase in conductivity up to 1 S m^{-1} was observed over 20 wt% PANI/DamCNCs, revealing the formation of a percolated particle network, resulting in a conductive material. **Figure S7** further evidenced the evolution in the conductivity from the change in the LED lamp intensity when connected to a low-frequency generator.

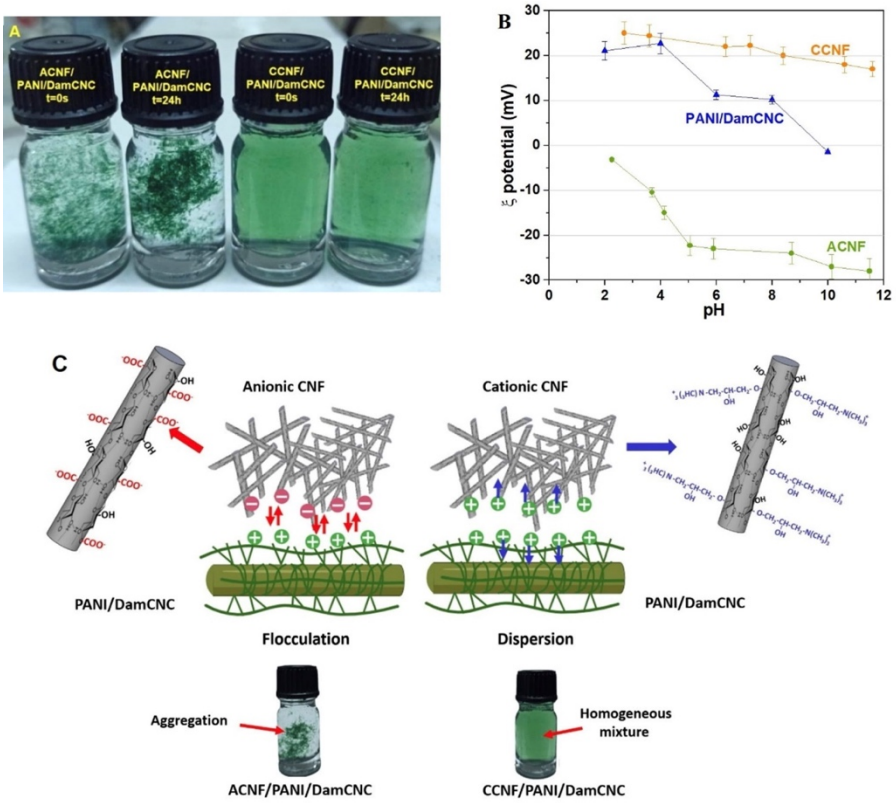

Figure 10: (A) ACNF-PANI/DamCNC and CCNF-PANI/DamCNC dispersions; (B) ζ-potential vs. pH of ACNF, CCNF, and PANI/DamCNC suspensions; (C) Simplified mechanism of the aggregation/dispersion of PANI/DamCNC and CNFs.

The difference in conduction properties of the nanopaper using ACNFs or CCNFs can be seen in **Figure 11C**, where the conductivity was plotted *vs.* the PANI/DamCNC content. The value of the DC conductivity increased abruptly to 10^{-2} S m^{-1} with the incorporation of 20 wt% PANI/DamCNCs loaded within the CCNF nanopaper. In addition, as the PANI/DamCNC loading increased, the conductivity of the nanopaper gradually improved. Beyond the percolation limit, a considerable change in conductivity was observed due to an increase in the number of conduction paths with potential contacts between PANI/DamCNC particles. This indicates that for a random distribution of PANI/DamCNCs, the setup of a conductive network above a critical concentration of added nanohybrid particles could be reached, resulting in an S-shape graph for conductivity vs. loading showing the three characteristic regimes: insulating, percolating and conductive (inset in **Figure 11C**). The formation of a conductive network among continuously connected PANI/DamCNCs was confirmed by the SEM images of the surface of a CCNF-PANI/DamCNC nanopaper containing 50 wt% PANI/DamCNCs (**Figure 12**). At high magnification, the surface appeared to be significantly coated by PANI particles. The conductivity achieved for CNFs containing over 40 wt% of PANI/DamCNCs is satisfactory for electronic applications and might be further improved by the addition of a doping agent.

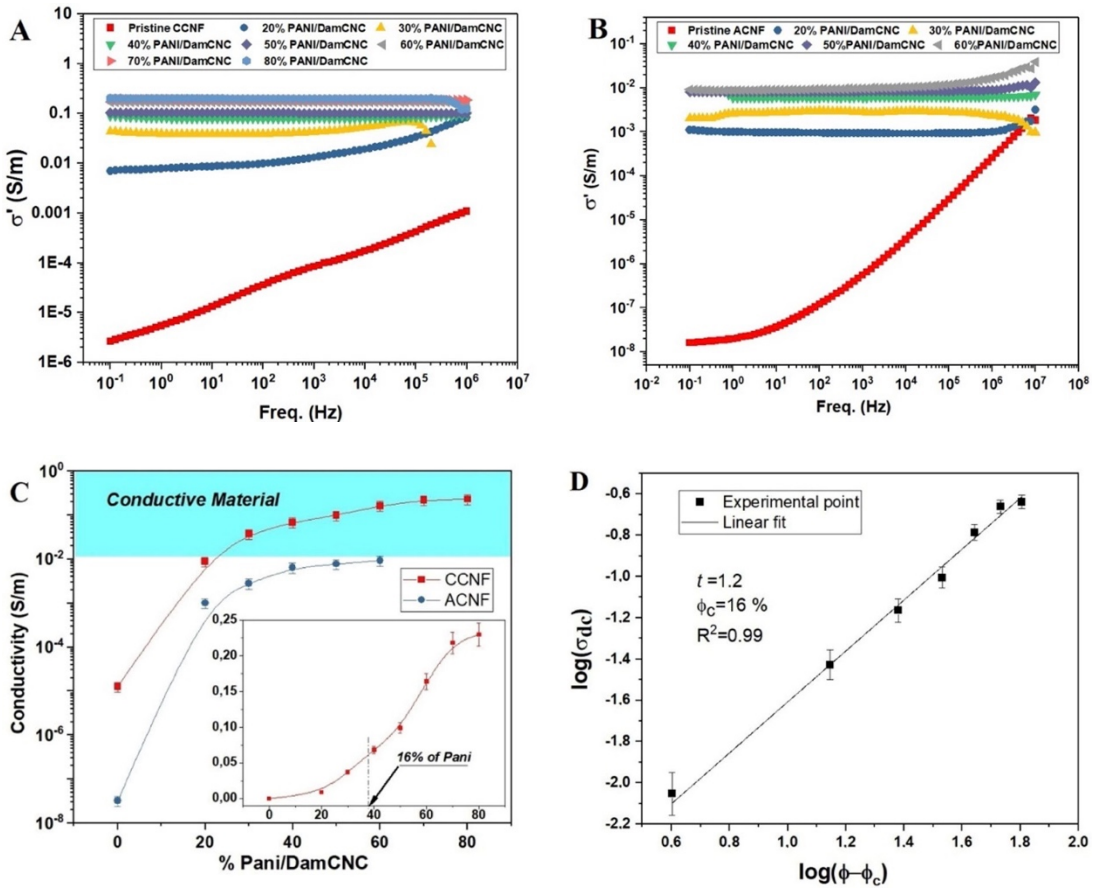

Figure 11: AC electrical conductivity vs. frequency for CCNF/PANI/DamCNC (A) and ACNF/PANI/DamCNC (B); (C) DC electrical conductivity for CNF/PANI/DamCNC films as a function of the PANI/DamCNC content; (D) linear fit of log σ_{dc} versus log($\phi - \phi_c$).

In addition to the critical type of CNFs (cationic *vs.* anionic) used in the preparation of the conductive nanopaper, the pH at which the nanopaper was prepared also plays a key role in controlling the conductivity. Indeed, in PANI-based materials, the conductivity strongly depended on pH and the highest conductivity was achieved only for the protonated form of PANI known as the emeraldine salt (ES) with a green color. Over pH 4, PANI tends to deprotonate, resulting in the formation of the non-conductive base emeraldine base (EB) form. This could be seen from the comparison of the conductivity of the nanopaper prepared from CCNFs and PANI/DamCNCs at a similar CNF-PANI/DamCNC ratio, but at a different pH of the mixture. Films prepared from a mixture at pH 2, exhibited a conductivity two orders of magnitude higher than the one prepared at pH 5 (**Figure S8**).

Interestingly, the addition of PANI/DamCNCs did not affect the mechanical performance of the films in terms of tensile modulus (E) and strength (S). Indeed, as shown in **Figure S9**, with increasing PANI/DamCNC, an enhancement in the strength of the film and E was observed, with a stronger effect on the strength. For instance, the neat CCNFs nanopaper achieved an E and S

around 2 GPa and 34 MPa, respectively. With the incorporation of 10 and 40 wt% DamCNCs, the E and S increased to 3 GPa/38 MPa, and 2.5 GPa/62 MPa, respectively. It is worth mentioning, that the levels of E and S were higher than those of tough and resistant polymers such as polyamide or polyesters, meaning that even from the mechanical point of view, this class of conductive nanopapers is competitive with polymers, with the merit of being sustainable, and biodegradable, as they originate from biomass resources.

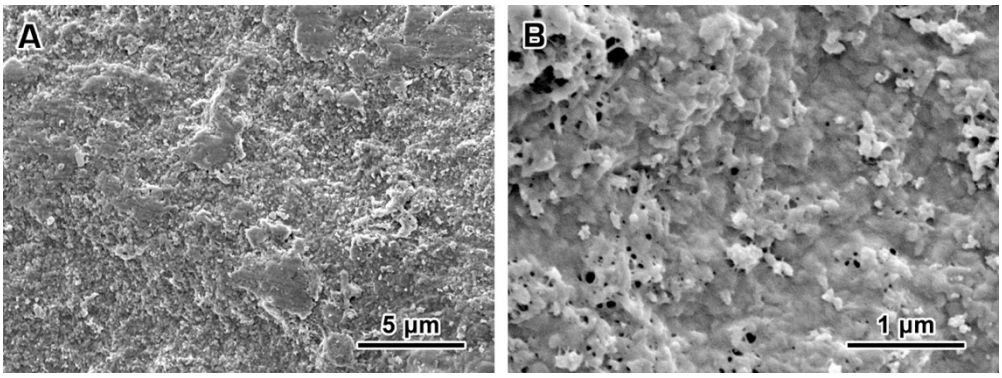

Figure 12: SEM images of the surface of a CCNF-PANI/DamCNC nanopaper containing 50 wt% of PANI/DamCNCs.

The conduction behavior throughout all three regimes was strongly affected by the composite structure. A lower filler loading limited the establishment of conductive paths throughout the filler, so no charge can flow and the composite remains non-conductive. By increasing the filler loading, the nanoparticles form a continuous network. Electrons can move along this network and the composite is conductive. Between these two extremes, conduction takes place when the fillers are not in direct contact but are connected via electron tunneling paths through an interface formed between the nanofiller and the matrix. In this case, the conductivity is lower than that of an interconnected network. This tunneling conduction is a quantum phenomenon where the contribution between the nearest neighbors is the most dominant [57].

To fit the experimental data of conductivity and to evaluate the percolation threshold for the CCNF-PANI/DamCNC composite, several literature reports used the power law equation of classical percolation theory given as follows [58]:

$$\sigma_{dc} = \sigma_0 \, (\phi - \phi_c)^t \quad \text{for } \phi > \phi_c \qquad \textbf{(2)}$$

where σ_{dc} is the DC conductivity of the composite, σ_0 is the conductivity of the polymer matrix, ϕ is the volume fraction of nanofiller, ϕ_c is the percolation threshold, and t is the critical exponent.

As shown in **Figure 11D**, the experimental data was well fitted by plotting $\log \sigma_{dc}$ *vs.* $\log(\phi - \phi_c)$. Theoretically, for ideal 2D percolation systems, the slope value t lies between 1.10

and 1.43. Accordingly, for the best linear fit of the data, the critical exponent *t* value was about 1.2 for the CCNF-PANI/DamCNC composites, revealing a quasi-two-dimensional network structure PANI/DamCNC nanohybrids within the CCNF scaffold. The conductivity value beyond a 16 wt% PANI loading marginally changed. The low percolation threshold revealed the successful formation of a continuous conductive network within the CCNF scaffold. As a result, the method of *in-situ* polymerization of PANI in the presence of DamCNCs was advantageous to achieve an effective PANI binding on the DamCNCs and consequently to prepare high electrically conductive CCNF films.

This approach to preparing thin conductive nanopapers was easy to implement using a papermaking process and water as the sole dispersion medium. The resulting thin films showed an acceptable conductivity around 1 S m^{-1} by adding only 20 wt% of PANI/DamCNCs, and without any additional post-treatment of the film. This opens the way toward the production of green flexible and lightweight electronic devices with broad potential applications in various fields such as optoelectronic devices, electronic displays, smart packaging, biomedical applications, or paper-based supercapacitors for energy storage. In addition, thanks to the good colloidal stability of CCNF-PANI/DamCNC systems and their nanosize, their use as conductive ink printers may be envisaged. The high thermal stability of PANI/DamCNCs below 200 °C and long-term robustness (mechanical stability of the film, toughness, permanent flexibility, absence of any visible change at rest for more than 6 months at room temperature and without any protection). Compared to another reported method for preparing conductive nanopapers based on the addition of carbon nanotubes, silver nanoparticles, and polymerization with polypyrrole [59], the present approach is easy to implement as it is based on the mixing of an already prepared suspension of PANI/DamCNCs to a CNF suspension. The flexibility and toughness, large surface area, and the fraction of conductive PANI of the resulting nanopapers were preserved, making them suitable for possible application in electromagnetic shielding, flexible supercapacitors, or electrodes for bio-battery applications.

3.9. Supercapacitor properties of CCNF-PANI/DamCNC nanopapers

To study the supercapacitor performance, the electrochemical analysis with a three-electrode system has emerged as an important strategy. A deeper understanding of supercapacitor electrodes was conducted, employing stainless steel-modified CCNFs, PANI/DamCNC, and their combinations CCNF-PANI/DamCNC nanopaper containing 50 wt% PANI/DamCNCs for working electrodes.

The CV curves CCNF/PANI-DamCNC 50% film at different scan rates from 2 to 100 $mV.s^{-1}$ in a 1 M H_2SO_4 electrolyte were shown in **Figure 13A**. All cyclic curves described a non-perfect

rectangular shape, indicating a diffusion-limited reversible capacitive performance of the system. In addition, the shape of the cyclic curve was well maintained even at a higher scan rate, showing its good performance. Furthermore, the current increased clearly with the rise of scan rates, indicating good rate capacity of the electrode materials.

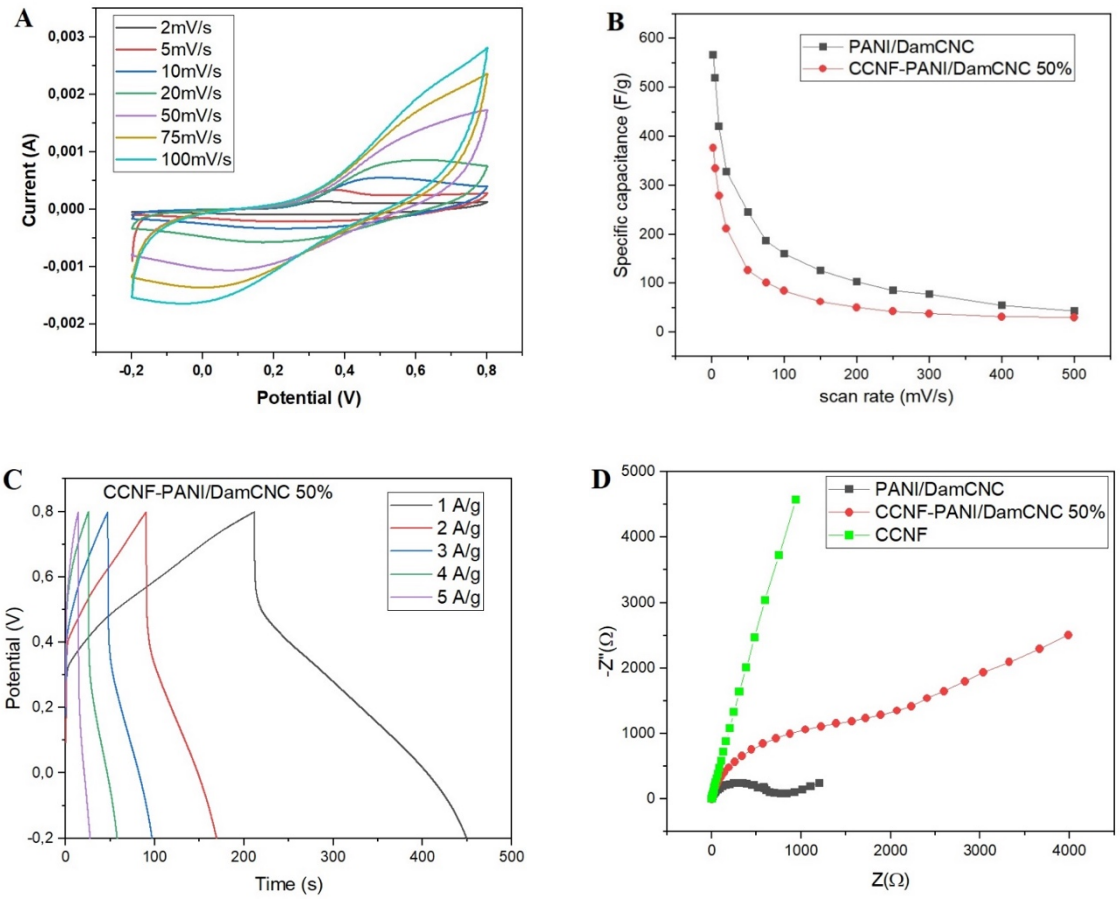

Figure 13: Electrochemical behavior of CCNF-PANI/DamCNC 50 %: CV curves at different scan rates (A) ; specific capacitances as a function of scan rate (B); charge−discharge curves at different current densities (C) and Nyquist plots of CCNFs, PANI/DamCNCs and the corresponding nanopaper with 50 wt% PANI/DamCNCs (D).

The variation of the specific capacitance for the nanocomposites as a function of the scan rate is shown in **Figure 13B**. As the scan rate increased, the diffusion rate of electrolytes from the solid/liquid interface to electrode materials failed to match the electrochemical reactions of the electrode materials at higher scan rates. Simultaneously, the protons reached the electrode surface and their entry into the active physical phase within a short scan cycle became difficult at higher scan rates, leading to reduced utilization of active materials. Consequently, the specific capacitance decreased with increasing scan rate, from 2 to 500 mV s^{-1}.

As depicted in **Figure 13B**, the CCNF-PANI/DamCNCs exhibited a specific capacity slightly weaker than that of PANI/DamCNC. This suggests that the PANI/DamCNC has a better ability to store and release electrical energy compared to the film composed of cellulose nanofibers and PANI/DamCNCs. This may be due to better accessibility of active sites in the material or improved electrical conductivity. Although the PANI/DamCNC showed a higher specific capacity, the CNF/PANI-CNC film offers superior flexibility and electrochemical characteristics similar to those of a pseudocapacitor, making it an interesting choice for certain specific applications.

Moreover, to assess the long-term performance and reliability of our pseudocapacitor electrodes, we conducted an extensive evaluation of capacitance retention. Subjecting to 500 CV cycles, the results of this cyclic testing revealed a remarkable minimum retention rate of over 60 % (**Figure S10**). This significant retention of capacitance underscores the excellent cyclic stability of the CCNF-PANI/DamCNC 50 % nanocomposite. These findings highlight the promising potential of CCNF-PANI/DamCNC nanopaper for real-world applications in various fields requiring reliable energy storage solutions.

We thoroughly examined the charge storage properties of our nanoper modified-electrode by conducting GCD measurements. **Figure 13C** showed the charge–discharge curves of the CCNF/PANI/DamCNC 50 % nanocomposite at different current densities within a potential window (–0.2 to 0.8 V *vs.* Ag/AgCl). GCD profiles of CCNF-PANI/DamCNC 50 % modified electrodes exhibited a distinctive non-linear shape with two voltage stages during discharge. At lower current densities of 1A g^{-1}, the initial stage (0.8–0.55 V) with a short discharge time suggested electrochemical double-layer capacitor behavior, while the subsequent stage (0.55 to -0.2 V)) with a longer discharge time indicated a combination the double layer capacitance and pseudocapacitive of PANI/DamCNC. Their areal capacitance can be calculated according to Equation 3,

$$C_a = \frac{I\,\Delta t}{m\,\Delta V} \qquad \textbf{(3)}$$

where I is the constant discharge current (A), t is the discharge time (s), ΔV is the potential window (V), and m is the mass (g) of the exposed working electrode. We noted that the areal capacitance of CCNF-PANI/DamCNC 50 % nanopaper can achieve a maximum value as high as 240 F g^{-1} at a current density of 1 A g^{-1} that is comparable to those of graphene oxide/PANI [60] and carbon nanotube /PANI [61].

To further determine the electronic/ionic conductivity of the corresponding nanopapers, the EIS was employed. The Nyquist impedance spectra of the modified electrodes are shown in **Figure 13D**. EIS plots of PANI/DamCNC and CCNF-PANI/DamCNC 50 % showed similar

curves including semicircle in the high-frequency region and a linear portion in the low-frequency region. Typically, the diameter of the arc reflects the charge transfer resistance associated with the electron-transfer-limited process between the electrodes and the electrolyte, while the intersection with the real axis in the high-frequency region represents the internal resistance arising from the intrinsic properties of the active materials and the electrolytic resistance. The CCNF curve showed a vertical line, meaning that pristine CCNF displays an ideal capacitive behavior.

It is worth noting that such prepared new material holds a significant promise for enhanced performance and a highly efficient, eco-friendly energy storage solution. By harnessing the high surface area and structural integrity of nanopaper alongside the conductivity of PANI and the reinforcing strength of DamCNCs, this unique combination confers to supercapacitors a higher capacitance, a greater stability and an improved durability. This innovative application opens doors to new possibilities in the field of energy storage devices, with potential applications in wearable electronics, electric vehicles, and renewable energy systems.

4. CONCLUSION

Dispersions with a high colloidal stability based on aniline polymerized in the presence of cellulose nanocrystals obtained by periodate oxidation and subsequent amination reduction were successfully prepared. The presence of the amine function contributed to the colloidal stability of DamCNCs suspensions, presumably through the preferential nucleation and growth of PANI on DamCNCs. TEM images have revealed distinct morphology of the nanohybrids: i) cylinders that may correspond to fully encapsulated CNC bundles and ii) star-like particles formed of PANI crystallites that grew radially with respect to the CNC surface. Upon drying of the suspensions, the formation of a continuous conductive network was attributed to the particle interaction via chemical and hydrogen bonding. These interactions were confirmed by FTIR and Raman spectra which indicated the appearance/disappearance of targeted functional groups after each chemical reaction carried out in this study. In addition, XRD and solid-state NMR analyses demonstrated the crystallinity of the formed PANI. These nanohybrids were incorporated into CNF scaffolds prepared from the same source as the aminated CNCs. The effective mixture of PANI/DamCNCs and CNFs resulted in thin and flexible nanopaper films using the pressurized filtration method. These films are environmentally friendly and biodegradable and exhibit multiresponsive properties through a simple, sustainable, and ecofriendly approach. that must be emphasized, as all the chemical reactions involved in the preparation of aminated CNCs and PANI/CNCs were carried out in water and were easy to run without any safety concerns.

The present work brought several novelties:

1) By introducing a functional group on the CNC surface, capable of chemically interacting with the growing PANI chains during the polymerization process, it was possible to control the morphology at the nanoscale of the PANI/CNC hybrid particles. This was demonstrated by comparing the morphology of PANI/CNCs prepared with neat or amine-functionalized CNCs.

2) The amine functionalization of CNCs using periodate-oxidation and amination with NH_4OH was a simple and effective approach to control the colloidal stability of the hybrid PANI/CNCs in water.

3) The hybridization of aminated CNCs with PANI has not been reported so far, opening the way toward better control of the morphology of PANI/CNCs, and the morphology of appended PANI in PANI/NC hybrid materials has never been described in detail in the literature. This aspect is of key importance for a perspective of the application of these materials.

4) We have shown the importance of the surface charge of the CNFs in producing stable suspensions of CNFs and hybrid PANI/CNCs for application in thin conductive nanopapers, where the PANI/CNCs were used as an additive to induce electrical conductivity without the addition of any extra dopant.

5) The mechanism inducing the grafting of PANI on DamCNCs was proposed, with emphasis on the key role of amine function on DamCNCs.

However, further work is needed to explain the presence of uncoated CNCs when DamCNCs were used. Possible reasons could be (i) an insufficient concentration of aniline during the polymerization process, (ii) an uneven distribution of the $-NH_2$ functions on the surface of DamCNCs, (iii) the peeling of the surface chains during the chemical modification of CNCs.

Acknowledgements

We thank the NanoBio-ICMG Platform (UAR 2607, Grenoble) for granting access to the NMR and Electron Microscopy facilities, as well as Patricia Chaud and Christine Lancelon-Pin (CERMAV) for the recording of NMR spectra and SEM images, respectively.

References

[1] S. Bhadra, D. Khastgir, N.K. Singha, J.H. Lee, Progress in preparation, processing and applications of polyaniline, Prog. Polym. Sci. 34 (2009) 783–810. https://doi.org/10.1016/j.progpolymsci.2009.04.003.

[2] D.A. Gopakumar, A.R. Pai, Y.B. Pottathara, D. Pasquini, L. Carlos de Morais, M. Luke, N. Kalarikkal, Y. Grohens, S. Thomas, Cellulose Nanofiber-Based Polyaniline Flexible Papers as Sustainable Microwave Absorbers in the X-Band, ACS Appl. Mater. Interfaces 10 (2018) 20032–20043. https://doi.org/10.1021/acsami.8b04549.

[3] F. Lodermeyer, M. Prato, R.D. Costa, D.M. Guldi, Facile and quick preparation of carbon nanohorn-based counter electrodes for efficient dye-sensitized solar cells, Nanoscale 8 (2016) 7556–7561. https://doi.org/10.1039/C6NR00629A.

[4] W. Hu, S. Chen, Z. Yang, L. Liu, H. Wang, Flexible Electrically Conductive Nanocomposite Membrane Based on Bacterial Cellulose and Polyaniline, J. Phys. Chem. B 115 (2011) 8453–8457. https://doi.org/10.1021/jp204422v.

[5] K. Lee, H. Yu, J.W. Lee, J. Oh, S. Bae, S.K. Kim, J. Jang, Efficient and moisture-resistant hole transport layer for inverted perovskite solar cells using solution-processed polyaniline, J. Mater. Chem. C 6 (2018) 6250–6256. https://doi.org/10.1039/C8TC01870G.

[6] R. Malik, S. Lata, R.S. Malik, Electrochemical behavior of composite electrode based on sulphonated polymeric surfactant (SPEEK/PSS) incorporated polypyrrole for supercapacitor, J. Electroanal. Chem. 835 (2019) 48–59. https://doi.org/10.1016/j.jelechem.2019.01.022.

[7] Y. Zhou, X. Liu, Z. Wang, M. Zhang, L. Yu, Y. Zhang, A novel PANI/SEBS film/fiber large deformation conductive elastomer with rapid recovery of resistance, Mater. Lett. 308 (2022) 131205. https://doi.org/10.1016/j.matlet.2021.131205.

[8] R. Nazar, A.A. Qaiser, U. Mehmood, M.S. Irfan, S. Sharif, Development of polyaniline/ethylene propylene diene monomer rubber (PANI/EPDM) conductive blend by in situ polymerization technique, J. Mater. Sci. Mater. Electron. 33 (2022) 14805–14815. https://doi.org/10.1007/s10854-022-08400-9.

[9] Y. Roichman, G.I. Titelman, M.S. Silverstein, A. Siegmann, M. Narkis, Polyaniline synthesis: influence of powder morphology on conductivity of solution cast blends with polystyrene, Synth. Met. 98 (1999) 201–209. https://doi.org/10.1016/S0379-6779(98)00190-8.

[10] L.F. Malmonge, G. de A. Lopes, S. do C. Langiano, J.A. Malmonge, J.M.M. Cordeiro, L.H.C. Mattoso, A new route to obtain PVDF/PANI conducting blends, Eur. Polym. J. 42 (2006) 3108–3113. https://doi.org/10.1016/j.eurpolymj.2006.08.002.

[11] R. Faez, W.A. Gazotti, M.-A. De Paoli, An elastomeric conductor based on polyaniline prepared by mechanical mixing, Polymer 40 (1999) 5497–5503. https://doi.org/10.1016/S0032-3861(98)00775-7.

[12] R.H. Cruz-Estrada, M.J. Folkes, IN-SITU PRODUCTION OF ELECTRICALLY CONDUCTIVE FIBRES IN POLYANILINE-SBS BLENDS, in: FRC 2000–Composites Millenn., Elsevier, 2000: pp. 238–245. https://doi.org/10.1533/9780857093134.238.

[13] S. Ray, A.J. Easteal, R.P. Cooney, N.R. Edmonds, Structure and properties of melt-processed PVDF/PMMA/polyaniline blends, Mater. Chem. Phys. 113 (2009) 829–838. https://doi.org/10.1016/j.matchemphys.2008.08.034.

[14] E. Ruckenstein, S. Yang, An emulsion pathway to electrically conductive polyaniline-polystyrene composites, Synth. Met. 53 (1993) 283–292. https://doi.org/10.1016/0379-6779(93)91097-L.

[15] X. Hong-Quan, M. Yong-Mei, G. Jun-Shi, Conductive polyaniline-SBS composites from in situ emulsion polymerization, Polymer (1998) 261–265.

[16] E. Ruckenstein, Y. Sun, Polyaniline-containing electrical conductive composite prepared by two inverted emulsion pathways, Synth. Met. 74 (1995) 107–113. https://doi.org/10.1016/0379-6779(95)03358-0.

[17] P.S. Rao, S. Subrahmanya, D.N. Sathyanarayana, Synthesis by inverse emulsion pathway and characterization of conductive polyaniline–poly(ethylene-co-vinyl acetate) blends, Synth. Met. 139 (2003) 397–404. https://doi.org/10.1016/S0379-6779(03)00192-9.

[18] P.S. Rao, D.N. Sathyanarayana, Inverted emulsion cast electrically conducting polyaniline-polystyrene blends, J. Appl. Polym. Sci. 86 (2002) 1163–1171. https://doi.org/10.1002/app.11059.

[19] X. Cheng, H. Wang, S. Wang, Y. Jiao, C. Sang, S. Jiang, S. He, C. Mei, X. Xu, H. Xiao, J. Han, Hierarchically core-shell structured nanocellulose/carbon nanotube hybrid aerogels for patternable, self-healing and flexible supercapacitors, J. Colloid Interface Sci. 660 (2024) 923–

933. https://doi.org/10.1016/j.jcis.2024.01.160.

[20] C. Sang, S. Wang, X. Jin, X. Cheng, H. Xiao, Y. Yue, J. Han, Nanocellulose-mediated conductive hydrogels with NIR photoresponse and fatigue resistance for multifunctional wearable sensors, Carbohydr. Polym. 333 (2024) 121947. https://doi.org/10.1016/j.carbpol.2024.121947.

[21] S.J. Eichhorn, A. Etale, J. Wang, L.A. Berglund, Y. Li, Y. Cai, C. Chen, E.D. Cranston, M.A. Johns, Z. Fang, G. Li, L. Hu, M. Khandelwal, K.-Y. Lee, K. Oksman, S. Pinitsoontorn, F. Quero, A. Sebastian, M.M. Titirici, Z. Xu, S. Vignolini, B. Frka-Petesic, Current international research into cellulose as a functional nanomaterial for advanced applications, J. Mater. Sci. 57 (2022) 5697–5767. https://doi.org/10.1007/s10853-022-06903-8.

[22] Y. Ko, G. Kwon, H. Choi, K. Lee, Y. Jeon, S. Lee, J. Kim, J. You, Cutting Edge Use of Conductive Patterns in Nanocellulose-Based Green Electronics, Adv. Funct. Mater. 33 (2023) 2302785. https://doi.org/10.1002/adfm.202302785.

[23] H. Sun, Y. Lu, Y. Chen, Y. Yue, S. Jiang, X. Xu, C. Mei, H. Xiao, J. Han, Flexible environment-tolerant electroluminescent devices based on nanocellulose-mediated transparent electrodes, Carbohydr. Polym. 296 (2022) 119891. https://doi.org/10.1016/j.carbpol.2022.119891.

[24] C.K. Maity, S. De, K. Verma, M. Moniruzzaman, S. Sahoo, Nanocellulose: A versatile nanostructure for energy storage applications, Ind. Crops Prod. 204 (2023) 117218. https://doi.org/10.1016/j.indcrop.2023.117218.

[25] Z. Niu, W. Cheng, M. Cao, D. Wang, Q. Wang, J. Han, Y. Long, G. Han, Recent advances in cellulose-based flexible triboelectric nanogenerators, Nano Energy 87 (2021) 106175. https://doi.org/10.1016/j.nanoen.2021.106175.

[26] N. Lin, A. Dufresne, Nanocellulose in biomedicine: Current status and future prospect, Eur. Polym. J. 59 (2014) 302–325. https://doi.org/10.1016/j.eurpolymj.2014.07.025.

[27] M.A.S. Azizi Samir, F. Alloin, A. Dufresne, Review of Recent Research into Cellulosic Whiskers, Their Properties and Their Application in Nanocomposite Field, Biomacromolecules 6 (2005) 612–626. https://doi.org/10.1021/bm0493685.

[28] T. Li, C. Chen, A.H. Brozena, J.Y. Zhu, L. Xu, C. Driemeier, J. Dai, O.J. Rojas, A. Isogai, L. Wågberg, L. Hu, Developing fibrillated cellulose as a sustainable technological material, Nature 590 (2021) 47–56. https://doi.org/10.1038/s41586-020-03167-7.

[29] S. Zhang, G. Sun, Y. He, R. Fu, Y. Gu, S. Chen, Preparation, Characterization, and Electrochromic Properties of Nanocellulose-Based Polyaniline Nanocomposite Films, ACS Appl. Mater. Interfaces 9 (2017) 16426–16434. https://doi.org/10.1021/acsami.7b02794.

[30] F. Tang, S. Li, H.-Y. Yu, C. Wang, Y. Li, Z. Li, J. Yao, J. Tang, J. Zhu, Tailoring Commercial Cellulose Membranes into Janus Conductive Electronic Skin via Diffusion-Controlled Polymerization, ACS Sustain. Chem. Eng. 8 (2020) 17458–17465. https://doi.org/10.1021/acssuschemeng.0c05913.

[31] X. Shi, L. Zhang, J. Cai, G. Cheng, H. Zhang, J. Li, X. Wang, A Facile Construction of Supramolecular Complex from Polyaniline and Cellulose in Aqueous System, Macromolecules 44 (2011) 4565–4568. https://doi.org/10.1021/ma2009904.

[32] Z. Zhou, X. Zhang, C. Lu, L. Lan, G. Yuan, Polyaniline-decorated cellulose aerogel nanocomposite with strong interfacial adhesion and enhanced photocatalytic activity, RSC Adv. 4 (2014) 8966. https://doi.org/10.1039/c3ra46441e.

[33] N. Lin, J. Huang, A. Dufresne, Preparation, properties and applications of polysaccharide nanocrystals in advanced functional nanomaterials: a review, Nanoscale 4 (2012) 3274. https://doi.org/10.1039/c2nr30260h.

[34] X. Wu, C. Lu, H. Xu, X. Zhang, Z. Zhou, Biotemplate Synthesis of Polyaniline@Cellulose Nanowhiskers/Natural Rubber Nanocomposites with 3D Hierarchical Multiscale Structure and Improved Electrical Conductivity, ACS Appl. Mater. Interfaces 6 (2014) 21078–21085. https://doi.org/10.1021/am505924z.

[35] G. Fei, Y. Wang, H. Wang, Y. Ma, Q. Guo, W. Huang, D. Yang, Y. Shao, Y. Ni, Fabrication of Bacterial Cellulose/Polyaniline Nanocomposite Paper with Excellent Conductivity, Strength, and Flexibility, ACS Sustain. Chem. Eng. 7 (2019) 8215–8225. https://doi.org/10.1021/acssuschemeng.8b06306.

[36] E. Ben Ayed, N. Ghorbel, A. Kallel, J.-L. Putaux, S. Boufi, Polyaniline-Grafted Chitin Nanocrystals as Conductive Reinforcing Nanofillers for Waterborne Polymer Dispersions, Biomacromolecules 23 (2022) 4167–4178. https://doi.org/10.1021/acs.biomac.2c00635.

[37] R. Koshani, J.E. Eiyegbenin, Y. Wang, T.G.M. van de Ven, Synthesis and characterization of hairy aminated nanocrystalline cellulose, J. Colloid Interface Sci. 607 (2022) 134–144. https://doi.org/10.1016/j.jcis.2021.08.172.

[38] A. Kumar, Y. Singh Negi, V. Choudhary, N. Kant Bhardwaj, Characterization of Cellulose Nanocrystals Produced by Acid-Hydrolysis from Sugarcane Bagasse as Agro-Waste, J. Mater. Phys. Chem. 2 (2020) 1–8. https://doi.org/10.12691/jmpc-2-1-1.

[39] I. Besbes, S. Alila, S. Boufi, Nanofibrillated cellulose from TEMPO-oxidized eucalyptus fibres: Effect of the carboxyl content, Carbohydr. Polym. 84 (2011) 975–983. https://doi.org/10.1016/j.carbpol.2010.12.052.

[40] A. Chaker, S. Boufi, Cationic nanofibrillar cellulose with high antibacterial properties, Carbohydr. Polym. 131 (2015) 224–232. https://doi.org/10.1016/j.carbpol.2015.06.003.

[41] B. Sun, Q. Hou, Z. Liu, Y. Ni, Sodium periodate oxidation of cellulose nanocrystal and its application as a paper wet strength additive, Cellulose 22 (2015) 1135–1146. https://doi.org/10.1007/s10570-015-0575-5.

[42] U.M. Casado, M.I. Aranguren, N.E. Marcovich, Preparation and characterization of conductive nanostructured particles based on polyaniline and cellulose nanofibers, Ultrason. Sonochem. 21 (2014) 1641–1648. https://doi.org/10.1016/j.ultsonch.2014.03.012.

[43] S. S., P. C., Development of Novel Polymer Nanostructures and Nanoscale Complex Hydrides for Reversible Hydrogen Storage, in: J. Liu (Ed.), Hydrog. Storage, InTech, 2012. https://doi.org/10.5772/50171.

[44] H. Tan, D. Xiao, R. Navik, Y. Zhao, Facile Fabrication of Polyaniline/Pristine Graphene–Bacterial Cellulose Composites as High-Performance Electrodes for Constructing Flexible All-Solid-State Supercapacitors, ACS Omega 6 (2021) 11427–11435. https://doi.org/10.1021/acsomega.1c00442.

[45] H. Luo, J. Dong, Y. Zhang, G. Li, R. Guo, G. Zuo, M. Ye, Z. Wang, Z. Yang, Y. Wan, Constructing 3D bacterial cellulose/graphene/polyaniline nanocomposites by novel layer-by-layer in situ culture toward mechanically robust and highly flexible freestanding electrodes for supercapacitors, Chem. Eng. J. 334 (2018) 1148–1158. https://doi.org/10.1016/j.cej.2017.11.065.

[46] D.L. VanderHart, R.H. Atalla, Studies of microstructure in native celluloses using solid-state carbon-13 NMR, Macromolecules 17 (1984) 1465–1472. https://doi.org/10.1021/ma00138a009.

[47] J. Leguy, A. Diallo, J.-L. Putaux, Y. Nishiyama, L. Heux, B. Jean, Periodate Oxidation Followed by $NaBH_4$ Reduction Converts Microfibrillated Cellulose into Sterically Stabilized Neutral Cellulose Nanocrystal Suspensions, Langmuir 34 (2018) 11066–11075. https://doi.org/10.1021/acs.langmuir.8b02202.

[48] F. Azzam, M. Galliot, J.-L. Putaux, L. Heux, B. Jean, Surface peeling of cellulose nanocrystals resulting from periodate oxidation and reductive amination with water-soluble polymers, Cellulose 22 (2015) 3701–3714. https://doi.org/10.1007/s10570-015-0785-x.

[49] T. Nypelö, B. Berke, S. Spirk, J.A. Sirviö, Review: Periodate oxidation of wood polysaccharides—Modulation of hierarchies, Carbohydr. Polym. 252 (2021) 117105. https://doi.org/10.1016/j.carbpol.2020.117105.

[50] A. Potthast, S. Schiehser, T. Rosenau, M. Kostic, Oxidative modifications of cellulose in the periodate system – Reduction and beta-elimination reactions 2 nd ICC 2007, Tokyo, Japan, October 25–29, 2007, Hfsg 63 (2009) 12–17. https://doi.org/10.1515/HF.2009.108.

[51] L.P. Novo, J. Bras, A. García, N. Belgacem, A.A.S. Curvelo, Subcritical Water: A Method for Green Production of Cellulose Nanocrystals, ACS Sustain. Chem. Eng. 3 (2015) 2839–2846. https://doi.org/10.1021/acssuschemeng.5b00762.

[52] E.S. Medeiros, L.H.C. Mattoso, R. Bernardes-Filho, D.F. Wood, W.J. Orts, Self-assembled films of cellulose nanofibrils and poly(o-ethoxyaniline), Colloid Polym. Sci. 286 (2008) 1265–1272. https://doi.org/10.1007/s00396-008-1887-x.

[53] Y. He, Preparation of polyaniline microspheres with nanostructured surfaces by a solids-stabilized emulsion, Mater. Lett. 59 (2005) 2133–2136. https://doi.org/10.1016/j.matlet.2005.02.047.

[54] A. Errokh, A. Magnin, J.-L. Putaux, S. Boufi, Morphology of the nanocellulose produced by periodate oxidation and reductive treatment of cellulose fibers, Cellulose 25 (2018) 3899–3911. https://doi.org/10.1007/s10570-018-1871-7.

[55] E. Song, J.-W. Choi, Conducting Polyaniline Nanowire and Its Applications in Chemiresistive Sensing, Nanomaterials 3 (2013) 498–523. https://doi.org/10.3390/nano3030498.

[56] Y. Wei, G.-W. Jang, K.F. Hsueh, E.M. Scherr, A.G. MacDiarmid, A.J. Epstein, Thermal transitions and mechanical properties of films of chemically prepared polyaniline, Polymer 33 (1992) 314–322. https://doi.org/10.1016/0032-3861(92)90988-9.

[57] S. Mondal, S. Ganguly, M. Rahaman, A. Aldalbahi, T.K. Chaki, D. Khastgir, N.Ch. Das, A strategy to achieve enhanced electromagnetic interference shielding at low concentration with a new generation of conductive carbon black in a chlorinated polyethylene elastomeric matrix, Phys. Chem. Chem. Phys. 18 (2016) 24591–24599. https://doi.org/10.1039/C6CP04274K.

[58] M.A. Munawar, D.W. Schubert, Highly Oriented Electrospun Conductive Nanofibers of Biodegradable Polymers-Revealing the Electrical Percolation Thresholds, ACS Appl. Polym. Mater. 3 (2021) 2889–2901. https://doi.org/10.1021/acsapm.0c01332.

[59] A.C. Baptista, I. Ropio, B. Romba, J.P. Nobre, C. Henriques, J.C. Silva, J.I. Martins, J.P. Borges, I. Ferreira, Cellulose-based electrospun fibers functionalized with polypyrrole and polyaniline for fully organic batteries, J. Mater. Chem. A 6 (2018) 256–265. https://doi.org/10.1039/C7TA06457H.

[60] R.R. Salunkhe, S. Hsu, K.C.W. Wu, Y. Yamauchi, Large-Scale Synthesis of Reduced Graphene Oxides with Uniformly Coated Polyaniline for Supercapacitor Applications, ChemSusChem 7 (2014) 1551–1556. https://doi.org/10.1002/cssc.201400147.

[61] D. Zha, P. Xiong, X. Wang, Strongly coupled manganese ferrite/carbon black/polyaniline hybrid for low-cost supercapacitors with high rate capability, Electrochimica Acta 185 (2015) 218–228. https://doi.org/10.1016/j.electacta.2015.10.139.

Supporting Information

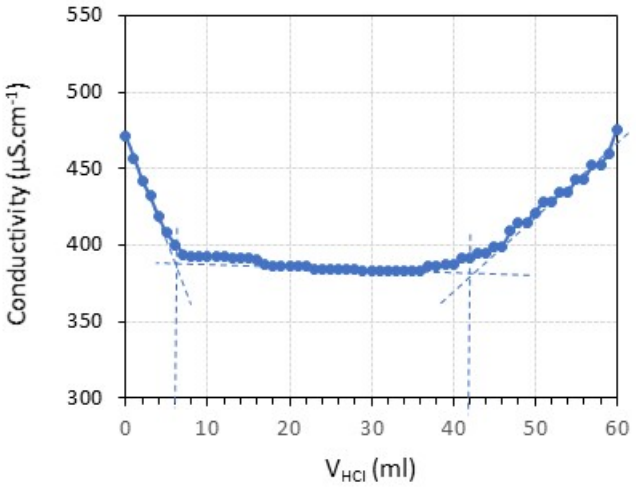

Figure S1. Conductometric titration of DamCNCs using HCl, 0.005 M: (m_{DamCNC} = 68 mg), indicating that ~36 ± 1 mL of acid is required to neutralize all the amino groups in DamCNCs, which corresponds to an amino content of ~2.6 mmol of $–NH_2$ per gram of DamCNCs.

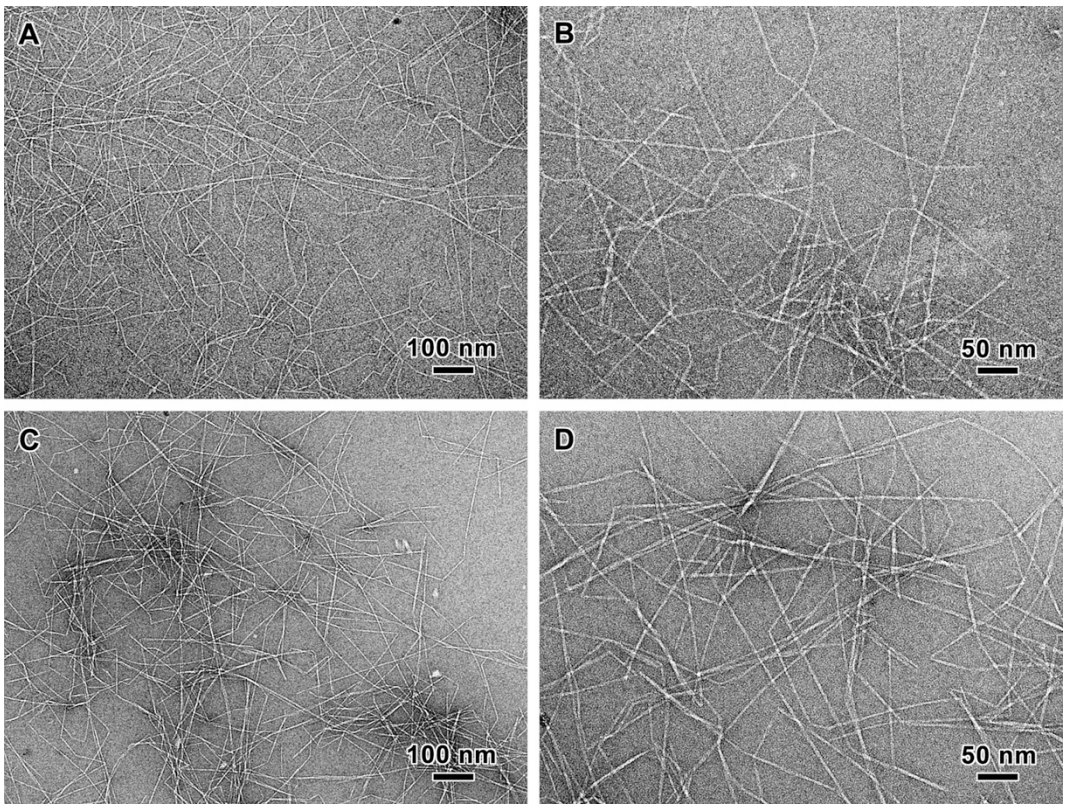

Figure S2. TEM micrographs of negatively stained ACNFs (A,B) and CCNFs (C,D).

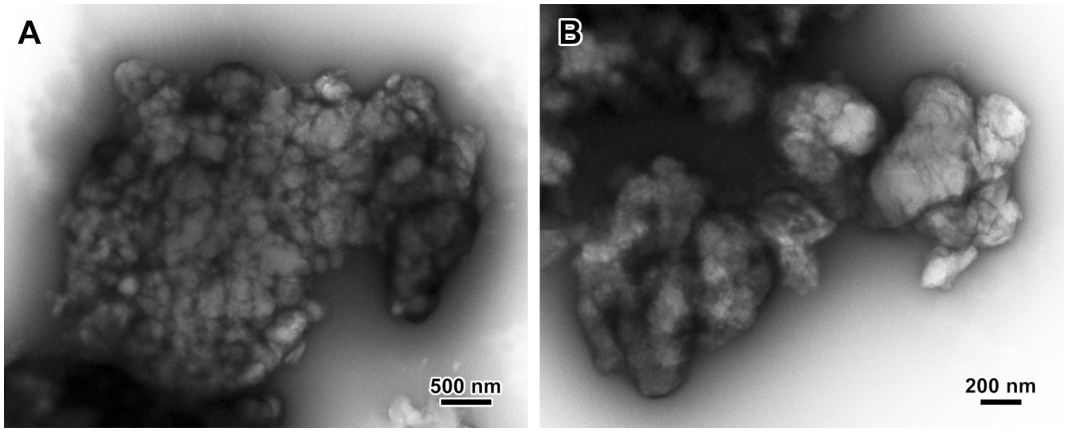

Figure S3. TEM images of negatively stained aggregates of PANI polymerized without CNCs.

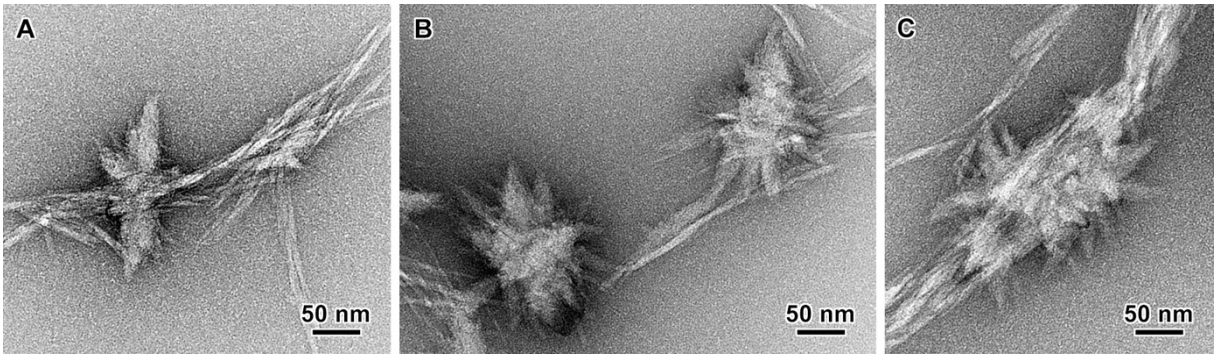

Figure S4. TEM images of negatively stained PANI/DamCNC particles.

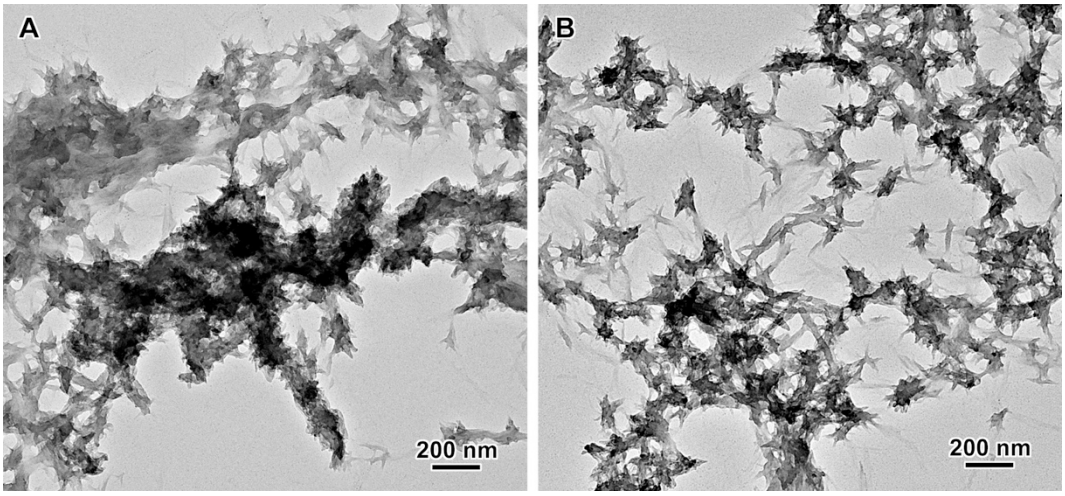

Figure S5. TEM images of an unstained preparation of PANI/DamCNCs.

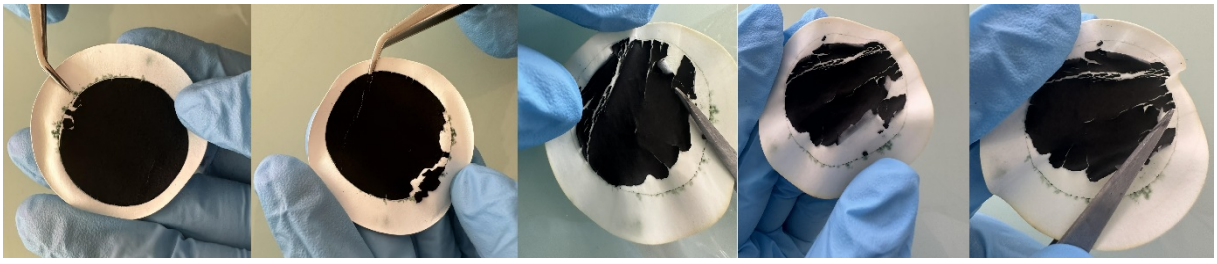

Figure S6. Photographs of a PANI/DamCNC film without CNFs lacking integrity and cohesion.

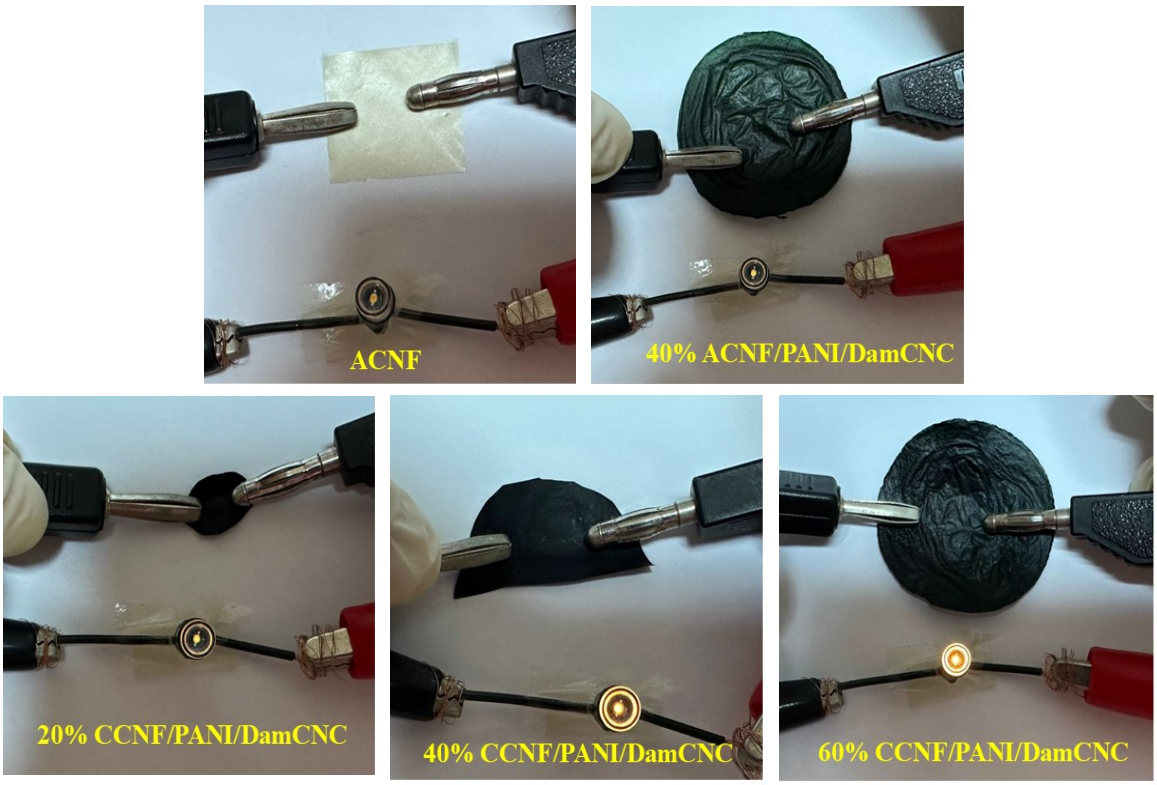

Figure S7. Conductivity demonstration of CNF-PANI/DamCNC at different DamCNC contents.

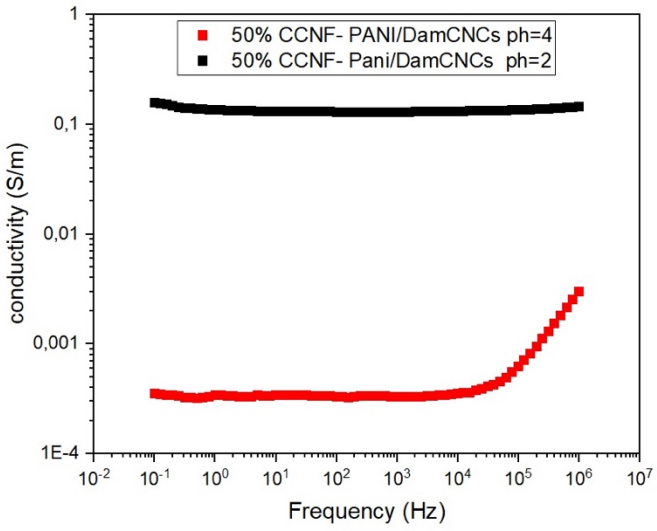

Figure S8. AC electrical conductivity *vs.* frequency for CCNF-PANI/DamCNC at different pH.

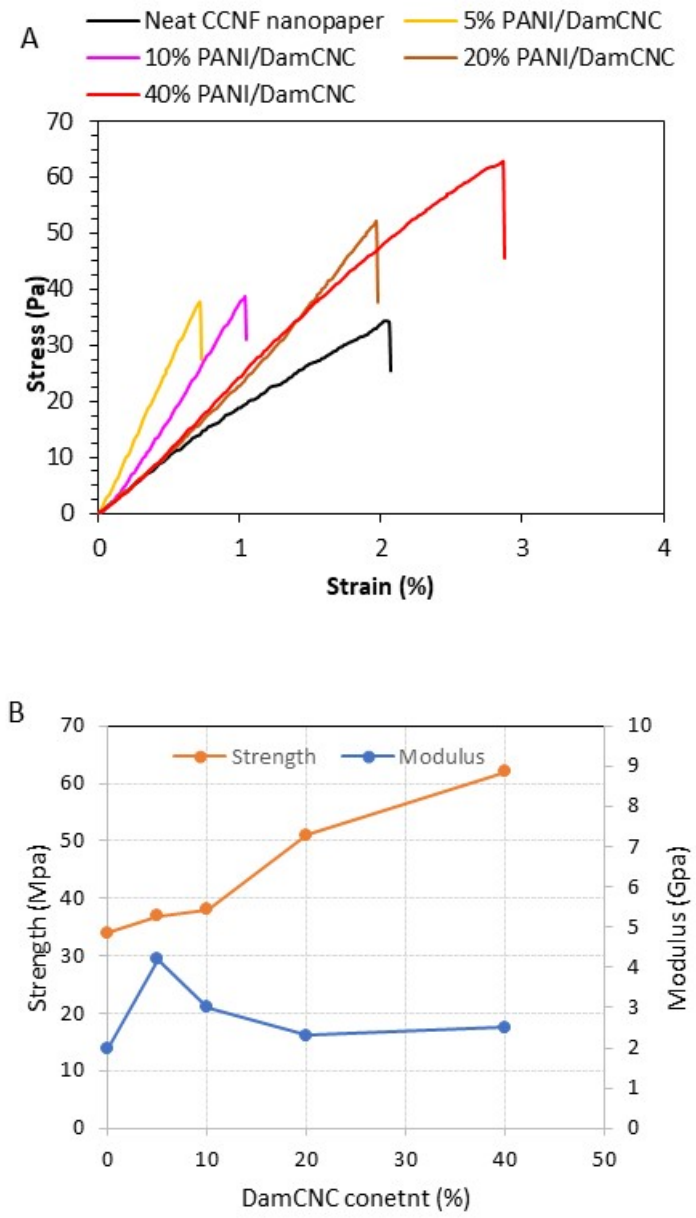

Figure S9. (A) Stress-strain trace for nanopaper from CCNFs at different contents in PANI/DamCNC, and (B) the corresponding strength and tensile modulus.

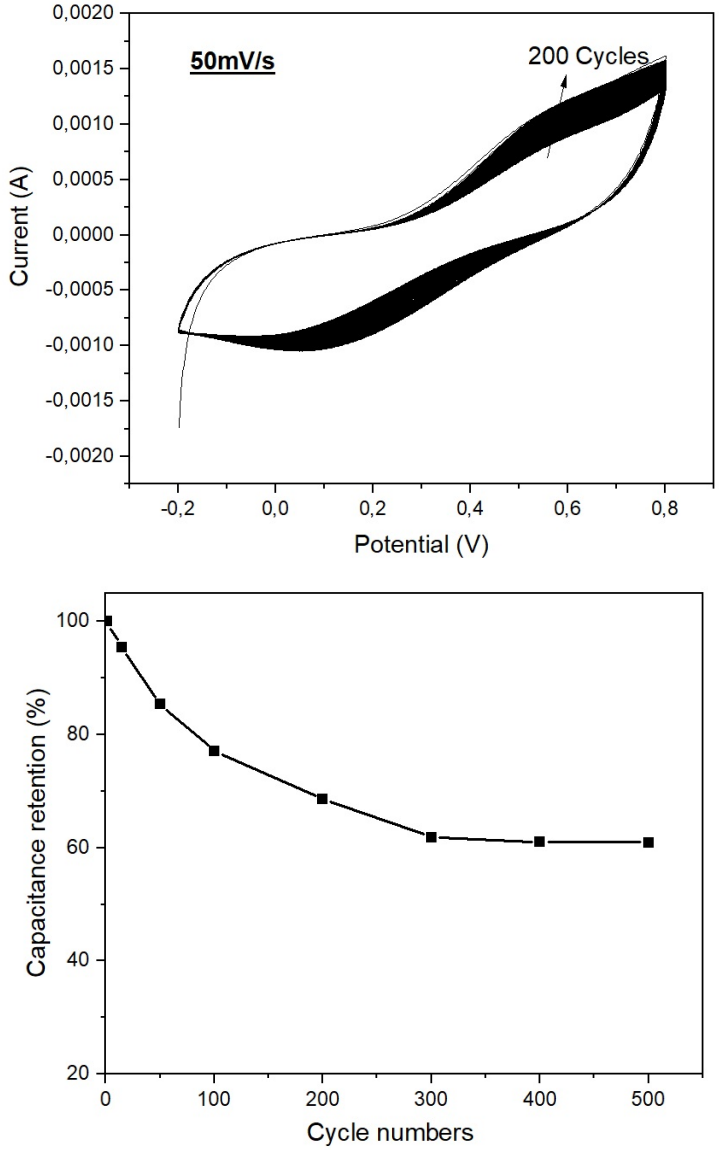

Figure S10. Cycle stability of CCNF-PANI/DamCNC 50 % measured at 50 mV s^{-1} for 500 cycles.